Top Heterocycl Chem (2006) 4: 107–159
DOI 10.1007/7081_024

Published online: 24 March 2006

Modeling Reaction Mechanism of Cocaine Hydrolysis and Rational Drug Design for Therapeutic Treatment of Cocaine Abuse

Chang-Guo Zhan

Department of Pharmaceutical Sciences, College of Pharmacy, University of Kentucky, 725 Rose Street, Lexington, KY 40536, USA
zhan@uky.edu

Abstract Cocaine is a widely abused heterocyclic drug and there is no available anti-cocaine therapeutic. The disastrous medical and social consequences of cocaine addiction have made the development of an effective pharmacological treatment a high priority. An ideal anti-cocaine medication would accelerate cocaine metabolism producing biologically inactive metabolites. The main metabolic pathway of cocaine in the body is hydrolysis at its benzoyl ester group. State-of-the-art molecular modeling of the reaction mechanism for the hydrolysis of cocaine and the mechanism-based design of anti-cocaine therapeutics will be discussed. First of all, competing reaction pathways and the transition state stabilization of the spontaneous hydrolysis of cocaine in solution will be examined. It will be demonstrated that the information obtained about the transition states and their stabilization has been very useful in the rational design of stable analogs of the transition states of cocaine hydrolysis, in order to elicit anti-cocaine catalytic antibodies. Detailed molecular modeling of the reaction mechanism for cocaine hydrolysis catalyzed by human butyrylcholinesterase (BChE), the primary cocaine-metabolizing enzyme in body, will be examined. Then, we will describe the application of these mechanistic insights to the rational design of human BChE mutants as a new therapeutic treatment of cocaine abuse. Finally, future directions of the mechanism-based design of anti-cocaine therapeutics will be discussed.

Keywords Cocaine · Hydrolysis mechanism · Transition-state simulation · Rational enzyme redesign · Catalytic antibody

Abbreviations

ACh	Acetylcholine
AChE	Acetylcholinesterase
BCh	Butyrylcholine
BChE	Butyrylcholinesterase
QM	Quantum mechanics
MM	Molecular mechanics
QM/MM	Quantum mechanics/molecular mechanics
MD	Molecular dynamics
BE	Benzoylecgonine
EME	Ecgonine methyl ester
CNS	Central nervous system
PET	Positron emission tomography
$B_{AC}2$	Base-catalyzed, acyl-oxygen cleavage, bimolecular
IRC	Intrinsic reaction coordinate
TSA	Transition state analog
TS	Transition state
TS1	Transition state for the first reaction step
TS2	Transition state for the second reaction step
TS3	Transition state for the third reaction step
TS4	Transition state for the fourth reaction step
INT	Intermediate
INT1	First intermediate
INT2	Second intermediate
INT3	Third intermediate
ES	Prereactive enzyme–substrate complex
SCRF	Self-consistent reaction field

SVPE	Surface and volume polarization for electrostatic interactions
FPCM	Fully polarizable continuum model
PCM	Polarizable continuum model
HBR	Hydrogen-bonded reactant complex
NPA	Natural population analysis
HBE	Hydrogen bonding energy
3D	Three-dimensional
ZPVE	Zero-point vibration energy

1 Introduction

1.1 Cocaine Abuse and Its Pharmacological Treatment

Cocaine is a widely abused heterocyclic drug (Fig. 1). Addiction and overdose of cocaine are major medical and public health problems that continue to defy treatment [1–3]. This drug molecule reinforces self-administration in relation to the peak serum concentration of the drug, the rate of rise to the peak, and the degree of change of the serum level. Potent central nervous system stimulation is followed by depression [4]. With overdose of the drug, respiratory depression, cardiac arrhythmia, and acute hypertension are common effects. The disastrous medical and social consequences of cocaine addiction (such as violent crime, loss in individual productivity, illness, and death) have made the development of an effective pharmacological treatment a high priority [5, 6].

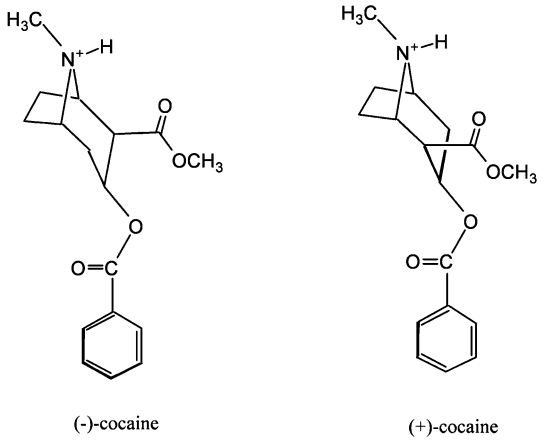

Fig. 1 Molecular structures of (–)-cocaine and (+)-cocaine

Pharmacological treatment for cocaine abuse and dependence can be either pharmacodynamic or pharmacokinetic. Most previously employed antiaddiction strategies use the classical pharmacodynamic approach, (i.e., developing small molecules that interact with one or more neuronal binding sites) with the goal of blocking or counteracting a drug's neuropharmacological actions. However, despite of decades of effort, existing pharmacodynamic approaches to cocaine abuse treatment have not yet proven successful [5–8].

1.2 Pharmacokinetic Approach

The inherent difficulties in antagonizing a blocker like cocaine have led to the development of a pharmacokinetic approach that aims at acting directly on the drug itself to alter its distribution or accelerate its clearance [7–14]. Pharmacokinetic antagonism of cocaine could be implemented by administration of a molecule, such as an anti-cocaine antibody, that binds tightly to cocaine so as to prevent it from crossing the blood–brain barrier [15–20].

The blocking action could also be implemented by administration of an enzyme or a catalytic antibody (regarded as an artificial enzyme) that not only binds but also accelerates cocaine metabolism and thereby frees itself for further binding [16–25]. Usually, a pharmacokinetic agent would not be expected to across the blood–brain barrier and thus would itself have no direct pharmacodynamic action, such as abuse liability [5].

1.3 Cocaine Metabolism

The primary pathway for metabolism of cocaine in primates is hydrolysis at the benzoyl ester or methyl ester group [5, 26]. Benzoyl ester hydrolysis generates ecgonine methyl ester (EME), whereas the methyl ester hydrolysis yields benzoylecgonine (BE). The major cocaine-metabolizing enzymes in humans are butyrylcholinesterase (BChE), which catalyzes benzoyl ester hydrolysis, and two liver carboxylesterases (denoted by hCE-1 and hCE-2), which catalyze hydrolysis at the methyl ester and the benzoyl ester, respectively. Of the three, BChE is the principal cocaine hydrolase in human serum. Hydrolysis accounts for about 95% of cocaine metabolism in humans. The remaining 5% is deactivated through oxidation by the liver microsomal cytochrome P450 system, producing norcocaine [5, 27]. EME appears the least pharmacologically active of the cocaine metabolites and may even cause vasodilation, whereas both BE and norcocaine appear to cause vasoconstriction and lower the seizure threshold, similarly to cocaine itself. Norcocaine is hepatotoxic and a local anesthetic [28]. Thus, hydrolysis of cocaine at the benzoyl ester by BChE is the pathway most suitable for amplification.

1.4 Butyrylcholinesterase

BChE, designated in older literature as pseudo-cholinesterase or plasma cholinesterase to distinguish it from its close cousin acetylcholinesterase (AChE), is synthesized in the liver and widely distributed in the body, including plasma, brain, and lung [5, 29]. Studies in animals and humans demonstrate that enhancement of BChE activity by administration of exogenous enzyme substantially decreases cocaine half-life [30–34]. For example, the addition of human BChE (extracted from donated blood) to human plasma containing cocaine (2 μg/mL) decreased the cocaine half-life in vitro from 116 min at a BChE concentration of 3.02 μg/mL to 10 min at a BChE concentration of 37.6 μg/mL. In vivo studies in animals have also revealed significant enhancement of BChE activity on cocaine's effects. Further, a single injection of the enzyme may increase plasma BChE activity for several days [5]. Clinical studies suggest that BChE has unique advantages. First, human BChE has a long history of clinic use, and no adverse effects have been noted with increased BChE plasma activity. Second, about 20 different naturally occurring mutants of human BChE have been identified [35], and there is no evidence that these mutants are antigenic. BChE also has potential advantages over active immunization since BChE administration would immediately enhance cocaine metabolism and would not require an immune response to be effective. For these reasons, enhancement of cocaine metabolism by administration of BChE is considered a promising pharmacokinetic approach for treatment of cocaine abuse and dependence [5, 6].

However, the catalytic activity of this plasma enzyme is three orders-of-magnitude lower against the naturally occurring (–)-cocaine than that against the biologically inactive (+)-cocaine enantiomer [36–39]. (+)-Cocaine can be cleared from plasma in seconds and prior to partitioning into the central nervous system (CNS), whereas (–)-cocaine has a plasma half-life of $\sim$ 45–90 min, long enough for manifestation of the CNS effects, which peak in minutes [21]. Thus, positron emission tomography (PET) applied to mapping of the binding of (–)-cocaine and (+)-cocaine in baboon CNS showed marked uptake corresponding to (–)-cocaine at the striatum along with other areas of low uptake, whereas no CNS uptake corresponding to (+)-cocaine was observed [37]. (+)-Cocaine was hydrolyzed by BChE so rapidly that it never reached the CNS for PET visualization. One may expect great progress in pharmacological treatment if a BChE mutant capable of hydrolyzing (–)-cocaine with the rate of (+)-cocaine hydrolysis by wild-type BChE is developed. Hence, BChE mutants with a significantly improved catalytic efficiency against (–)-cocaine are highly desirable for use as an exogenous enzyme in humans. As discussed below, encouraging progress has been made in recent computational design of high-activity mutants of human BChE.

2
Mechanism for Non-enzymatic Hydrolysis of Cocaine

Anti-cocaine catalytic antibodies are a novel class of artificial enzymes with unique potential as therapeutic agents for cocaine overdose and addiction [21, 22]. This novel class of artificial enzymes, elicited by immunization with transition-state analogs of cocaine benzoyl-ester hydrolysis, have unique potential as therapeutic artificial enzymes due to their biocompatibility and extended plasma half-life. The design of a transition-state analog that would elicit a catalytic antibody [40] is based on the mechanism of the corresponding non-enzymatic reaction, specifically the transition-state structure for the rate-determining step. Hence, a more complete understanding of the mechanism of cocaine hydrolysis in aqueous solution could provide additional insights into the rational design of more effective transition-state analogs. This is why computational studies for development of anti-cocaine catalytic antibodies have been focused on the reaction coordinate calculations on the detailed mechanisms for non-enzymatic hydrolysis of cocaine in water.

2.1
Hydrolysis of Cocaine Free Base

As one can see from Fig. 1, cocaine has two carboxylic acid ester groups: benzoyl ester and methyl ester. Hence, the fundamental reaction pathway for non-enzymatic hydrolysis of cocaine at both benzoyl ester and methyl ester groups is expected to be similar to that for the usual non-enzymatic hydrolysis of a carboxylic acid ester. The hydrolysis of the majority of common alkyl esters, RCOOR′, in neutral solution occurs through attack at the hydroxide ion at the carbonyl carbon [41–48]. This mode of hydrolysis has been designated as $B_{AC}2$ (base-catalyzed, acyl-oxygen cleavage, bimolecular) [43], and is believed to occur by a two-step mechanism, although a concerted pathway can arise in the case of esters containing very good leaving groups (corresponding to a low pK_a value for R′OH) [49–56]. The generally accepted two-step mechanism consists of the formation of a tetrahedral intermediate (first step), followed by decomposition of the tetrahedral intermediate to yield products $RCOO^-$ + R′OH (second step) [43]. Degradation of cocaine may take place through the $B_{AC}2$ route of hydrolysis of either the benzoyl ester group or the methyl ester group.

The earliest theoretical calculations of cocaine hydrolysis focused on the first step of the hydrolysis of the benzoyl ester [57, 58]. In these computational studies [57, 58], MNDO, AM1, PM3, and SM3 semiempirical molecular orbital methods, as well as ab initio procedure at the HF/3-21G level of theory, were employed to optimize geometries of the transition states for the first step of the hydrolysis of cocaine and model esters, including methyl acetate [59, 60] for which experimental activation energy in aqueous solu-

tion is available. However, the geometry optimization of the first transition state for the cocaine benzoyl-ester hydrolysis was successful with only the MNDO, PM3, and SM3 methods. No first-order saddle point corresponding to the expected transition state structure was found on the AM1 and HF/3-21G potential energy surfaces. Thus, it was necessary to further examine this putative transition state with higher levels of theory. Further, the energy barrier, 24.6 kcal/mol [57], predicted by the semiempirical molecular orbital calculations for the first step of the hydrolysis of neutral cocaine in aqueous solution was likely overestimated, as the energy barrier, 23.4 kcal/mol [59, 60], determined by the same kind of calculations for the first step of the methyl acetate hydrolysis was significantly larger than the reported experimental activation energy, 10.45 kcal/mol [61] or 12.2 kcal/mol [62], in aqueous solution.

As discussed below in detail, first-principles electronic structure calculations have provided accurate predictions of the reaction pathways and the corresponding energy barriers, not only for the first step of hydrolysis of cocaine free base at the benzoyl ester group, but also for the entire reaction processes of hydrolysis of cocaine free base at both the benzoyl ester and methyl ester groups.

2.1.1 Geometries of Transition States and Intermediates

In a more sophisticated computational study [63], first-principles reaction coordinate calculations on the hydrolysis of cocaine free base (neutral cocaine) were performed by using Becke's three-parameter hybrid exchange functional [64] and the Lee–Yang–Parr correlation functional (B3LYP) [65] with the 6-31+G(d) basis set. Vibrational frequencies were evaluated at the optimized geometries to confirm all the first-order saddle points and local minima found on the potential energy surfaces, and to evaluate zero-point vibration energies (ZPVE). Intrinsic reaction coordinate (IRC) calculations [66, 67] were also performed to verify the expected connections of the first-order saddle points with local minima found on the potential energy surfaces [63]. The important geometries optimized at the B3LYP/6-31+G(d) level for the base-catalyzed hydrolysis of neutral cocaine and three model esters are depicted in Figs. 2 and 3 [63]. The reaction coordinate calculations indicate that the mechanisms of the base-catalyzed hydrolysis of the cocaine benzoyl ester and methyl ester groups are indeed similar to the usual two-step $B_{AC}2$ route of hydrolysis of alkyl esters [43, 47]. The first step is the formation of a tetrahedral intermediate by the attack of hydroxide oxygen at the carbonyl carbon of cocaine methyl ester or benzoyl ester group. The second step is the decomposition of the tetrahedral intermediate to products through breaking the C – O bond between the carbonyl carbon and ester oxygen [63].

For the cocaine benzoyl ester hydrolysis, the nucleophilic hydroxide ion can approach from the two faces, denoted by Re and Si, of the carbonyl to

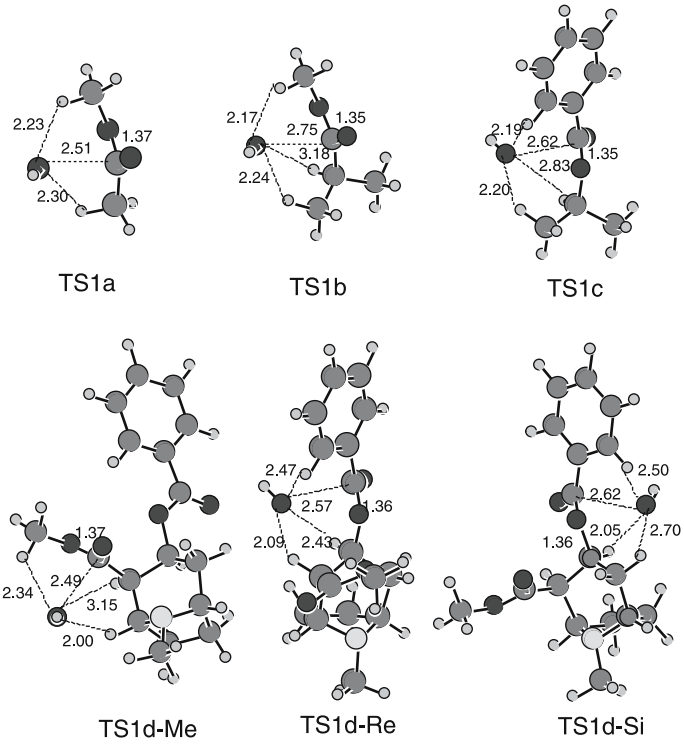

Fig. 2 Geometries of the transition states optimized at the B3LYP/6-31+G(d) level for the first step of the hydrolysis of CH_3COOCH_3, $(CH_3)_2CHCOOCH_3$, $C_6H_5COOCH(CH_3)_2$, the cocaine methyl-ester, and the cocaine benzoyl-ester [63]. Internuclear distances are given in angstrom

form two stereoisomer tetrahedral intermediates (*S* and *R*). The two transition state structures, denoted by TS1d-Re and TS1d-Si, optimized at the B3LYP/6-31+G(d) level for the two competing pathways of the first step of the cocaine benzoyl-ester hydrolysis are depicted in Fig. 2, together with those optimized for the first step of the hydrolysis of CH_3COOCH_3 (TS1a), $(CH_3)_2CHCOOCH_3$ (TS1b), $C_6H_5COOCH(CH_3)_2$ (TS1c), and the cocaine methyl-ester (TS1d-Me) [63]. As one can see from Fig. 2, all of the six transition state structures for the first step are very similar to each other as far as the position of the nucleophilic hydroxide relative to the carbonyl. The distances between the hydroxide oxygen and carbonyl carbon are 2.49–2.75 Å.

As the second step of the ester hydrolysis, the decomposition of the tetrahedral intermediate requires a proton transfer from the hydroxide/hydroxyl oxygen to the ester oxygen, while the C – O bond between the carbonyl carbon and ester oxygen gradually breaks. Two competing pathways were examined for the second step [63]: one associated with the direct proton

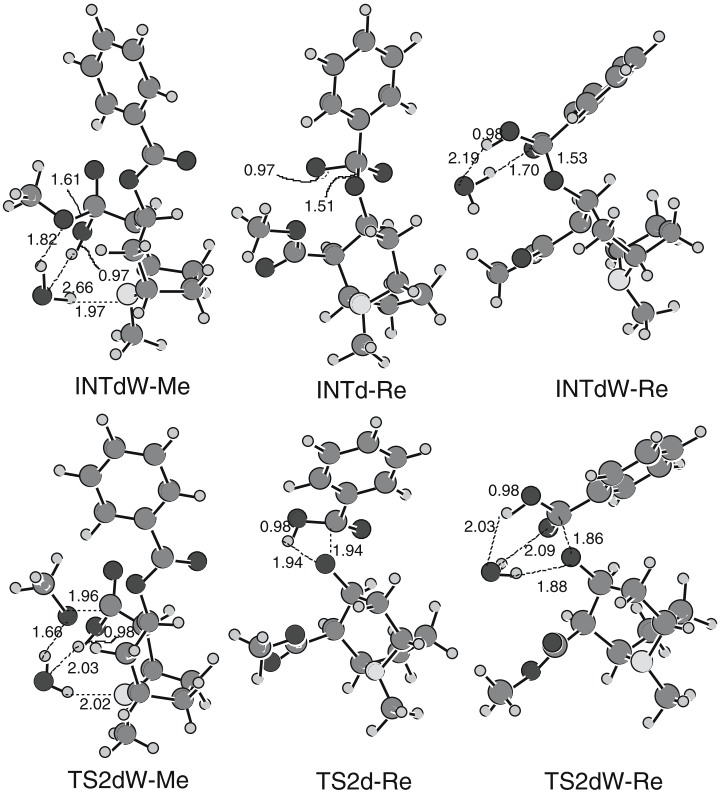

Fig. 3 Geometries of the second transition states and the corresponding tetrahedral intermediates optimized at the B3LYP/6-31+G(d) level for the hydrolysis of the cocaine methyl-ester and benzoyl-ester groups [63]. Internuclear distances are given in angstrom

transfer from the hydroxide/hydroxyl oxygen to the ester oxygen; and the other associated with a water-assisted proton transfer. Figure 3 depicts the optimized geometries of the transition state for the water-assisted proton transfer (TS2dW-Me) during the cocaine methyl-ester hydrolysis and the transition states for the direct proton transfer (TS2d-Re) and water-assisted proton transfer (TS2dW-Re) during the cocaine benzoyl-ester hydrolysis initialized by the hydroxide attack from the Re face. Figure 3 also shows the optimized geometries of the tetrahedral intermediates INTdW-Me, INTd-Re, and INTdW-Re corresponding to transition states TS2dW-Me, TS2d-Re, and TS2dW-Re, respectively. For the water-assisted proton transfer pathway involving transition state TS2dW-Re (or TS2dW-Me), the water molecule hydrogen-bonding with the ester oxygen in the tetrahedral intermediate INTdW-Re (or INTdW-Me) gradually transfers a proton to the ester oxygen through the hydrogen bond, while the hydroxide/hydroxyl proton gradually transfers to the water oxygen.

2.1.2 Energy Barriers for the Formation of the Tetrahedral Intermediates

The geometries optimized at the B3LYP/6-31+G(d) level were employed to carry out the single-point energy calculations at the MP2/6-31+G(d) level [63]. Solvent shifts of the energies were accounted for by performing self-consistent reaction field (SCRF) energy calculations using the geometries optimized at the B3LYP/6-31+G(d) level in gas phase. The energy barrier for reaction in aqueous solution was taken as a sum of the energy change calculated at the MP2/6-31+G(d)//B3LYP/6-31+G(d) level in gas phase and the corresponding solvent shift determined by the SCRF calculations at the HF/6-31+G(d) level.

The solute–solvent interaction can be divided into a long-range electrostatic interaction and short-range non-electrostatic interactions (such as cavitation, dispersion, and Pauli repulsion) [68–72]. The dominant long-range electrostatic interaction was evaluated by using the GAMESS [73] implementation of the surface and volume polarization for electrostatic interactions (SVPE) [74–76]. The SVPE model is also known as the fully polarizable continuum model (FPCM) [47, 48, 63, 77–89] because it fully accounts for both surface and volume polarization effects in the SCRF calculation. The contributions of short-range non-electrostatic interactions to the energy barriers were estimated by using the polarizable continuum model (PCM) [68] implemented in the Gaussian98 program [90] with the default choices of the program for the recommended standard parameters. The total solvent shift [63] was taken as a sum of the long-range electrostatic interaction contribution determined by the SVPE calculation and the total contribution of the short-range non-electrostatic interactions determined by the PCM calculation.

The energy barriers determined for the ester hydrolyses in aqueous solution are summarized in Table 1. The total energy of the individual reactants, $RCOOR' + HO^-$, in gas phase is about 14–26 kcal/mol higher than the first transition state (TS1). Theoretical studies of the alkaline hydrolysis of alkyl esters revealed that for the ester hydrolysis in gas phase, between the individual reactants and TS1, there is a hydrogen-bonded reactant complex (denoted by HBR) [46] whose energy is lower than TS1. Thus, the energy barrier for the first step of the hydrolysis, i.e., formation of the tetrahedral intermediate, in gas phase is the energy change from HBR to TS1. However, in aqueous solution various SCRF calculations gave the same qualitative result that the individual reactants are more stable than both TS1 and HBR, whereas HBR is still more stable than TS1 [47]. It follows that in aqueous solution the HBR structure is not stable, and that the reaction goes directly from the individual reactants to TS1. This is because the interaction between solvent water and the individual reactants is stronger than that between methyl acetate and hydroxide ion. Hence, the energy barrier for the first step of the hydrolysis in

Table 1 Energy barriers (in kcal/mol) calculated for the base-catalyzed hydrolysis of neutral cocaine and model esters in aqueous solution [63] [a]

Reaction	ΔE(Gas) [b]	Solvent shift [c] Electrostatic (SVPE)	Non-electrostatic (PCM) [e]	Total	Energy barrier
CH_3COOCH_3					
Reactants → TS1a	– 14.31	25.15 [24.98] [d]	0.52	25.67	11.4 [f]
$(CH_3)_2CHCOOCH_3$					
Reactants → TS1b	– 14.05	20.97	1.05	22.02	8.0
$C_6H_5COOCH(CH_3)_2$					
Reactants → TS1c	– 19.16	26.69	1.32	28.00	8.8
Cocaine (methyl-ester)					
Reactants → TS1d-Me	– 18.68	24.81	0.84	25.65	7.0
INTdW-Me → TS2dW-Me	2.51	2.51	– 0.23	2.28	4.8
Cocaine (benzoyl-ester)					
Reactants → TS1d-Re	– 26.33	32.40	1.55	33.95	7.6
Reactants → TS1d-Si	– 22.99	30.26	1.25	31.51	8.5
INTd-Re → TS2d-Re	3.52	7.49	1.37	8.86	12.4
INTdW-Re → TS2dW-Re	2.16	1.32	– 0.33	0.99	3.2

[a] All calculations used geometries optimized at the B3LYP/6-31+G(d) level in gas phase
[b] Energy change determined at the MP2/6-31+G(d)//B3LYP/6-31+G(d) level in gas phase. The ZPVE corrections were made for all the values
[c] Unless otherwise indicated, the solvent shifts were determined by performing the SVPE and PCM calculations at the HF/6-31+G(d) level
[d] Values in brackets were determined by carrying out the SVPE calculations at the MP2/6-31+G(d) level
[e] Total contribution of non-electrostatic interactions between solute and solvent
[f] The corresponding experimental activation energies reported for hydrolysis of CH_3COOCH_3 in aqueous solution were 10.45 kcal/mol [61] and 12.2 kcal/mol [62]

aqueous solution is the energy change from the individual solvated reactants to the solvated first transition state TS1. As shown in Table 1, the extremely large solvent shifts of the energy barriers for the first step of the ester hydrolysis are attributed mainly to the contributions of the long-range electrostatic interactions between the solutes and solvent.

As one can see from Table 1, the solvent shift determined for the first step of the hydrolysis of methyl acetate (the rate-determining step) by the SVPE calculations at the MP2/6-31+G(d) level differs from the shift determined at the HF/6-31+G(d) level by less than 0.2 kcal/mol. The calculated energy barrier, 11.4 kcal/mol, is in good agreement with the experimental determinations of activation energy, 10.45 or 12.2 kcal/mol, reported for the hydrolysis of methyl acetate in aqueous solution [61, 62].

As seen in Table 1, the energy barrier, 7.6 kcal/mol, calculated for the first step of the cocaine benzoyl ester hydrolysis through the hydroxide attack from the Re face of the carbonyl is ~ 1 kcal/mol lower than that through hydroxide attack from the Si face. The energy barrier, 7.0 kcal/mol, calculated for the first step of the cocaine methyl ester hydrolysis is slightly lower than the lowest barrier, 7.6 kcal/mol, for the first step of the cocaine benzoyl-ester hydrolysis. The energy barriers calculated for the first step of the cocaine hydrolysis are all significantly lower than the barrier for the first step of the hydrolysis of methyl acetate. To understand the changes of the calculated energy barriers from methyl acetate hydrolysis to cocaine hydrolysis, the cocaine hydrolysis will be compared with the hydrolysis of other two simplified cocaine models, $(CH_3)_2CHCOOCH_3$ and $C_6H_5COOCH(CH_3)_2$, representing the cocaine methyl-ester and benzoyl-ester, respectively.

Methyl acetate, CH_3COOCH_3, is a minimal model of the cocaine methyl ester in which the two β carbon atoms for the carboxylic acid moiety of the methyl ester are all simplified as hydrogen atoms. $(CH_3)_2CHCOOCH_3$ is a slightly larger model of the cocaine methyl ester in which the two β carbon atoms for the carboxylic acid moiety of the cocaine methyl ester are represented as methyl groups. Correspondingly, transition state structures TS1a and TS1b may be regarded as two simplified models of transition state structure TS1d-Me, as seen in Fig. 2. The energy barrier, 8.0 kcal/mol, calculated for the $(CH_3)_2CHCOOCH_3$ hydrolysis is 3.4 kcal/mol lower than that for the CH_3COOCH_3 hydrolysis but matches cocaine methyl ester hydrolysis very well at only 1.0 kcal/mol higher. It follows that substitution of the two α hydrogen atoms in R with two methyl groups significantly decreases the energy barrier for the first step of the ester hydrolysis, and that further substitution of the β hydrogen for the carboxylic acid moiety slightly decreases the energy barrier. The significant decrease of the energy barrier upon substitution of the two α hydrogen atoms in R with two methyl groups may be attributed mainly to the stronger C – H ··· O hydrogen bond [91–93] between the hydroxide oxygen and one of the β hydrogen atoms in the first transition state (TS1b or TS1d-Me). The fact that the hydrogen bond with the β hydrogen is stronger than the hydrogen bond with the α hydrogen is caused by the steric effect. In the transition state, the β hydrogen is sterically more favorable than the α hydrogen to form a hydrogen bond with the hydroxide oxygen. Thus, $(CH_3)_2CHCOOCH_3$ is a reasonable model for the cocaine methyl ester. Similarly, $C_6H_5COOCH(CH_3)_2$ models the cocaine benzoyl ester in which the two β carbon atoms for the alcohol moiety of the cocaine benzoyl ester are represented as methyl groups. Correspondingly, transition state structure TS1c may be regarded as a model of transition state structure TS1d-Re. The energy barrier, 8.8 kcal/mol, calculated for the $C_6H_5COOCH(CH_3)_2$ hydrolysis is very close to that of the cocaine benzoyl ester (TS1d-Re) at only 1.2 kcal/mol higher. Thus, $C_6H_5COOCH(CH_3)_2$ is a reasonable model for the cocaine benzoyl-ester.

2.1.3
Energy Barriers for the Decomposition of the Tetrahedral Intermediates

The energy barrier for the second step of the cocaine hydrolysis, i.e., decomposition of the tetrahedral intermediate, is the energy change from the intermediate (INT) to the second transition state (TS2) no matter whether the hydrolysis occurs in gas phase or in aqueous solution. The energy barriers were also determined by using the same computational protocol described above. Since the calculated energy barrier for the first step of the hydrolysis associated with transition state TS1d-Re is lower than that associated with transition state TS1d-Si, the whole reaction pathway, individual reactants → TS1d-Re → INTd-Re → TS2d-Re → individual products, was considered only for the cocaine benzoyl ester hydrolysis involving the direct proton transfer. The energy barrier, 12.4 kcal/mol, calculated for the second step of the hydrolysis associated with transition state TS2d-Re is 4.8 kcal/mol higher than the corresponding first step. For the cocaine benzoyl-ester hydrolysis involving the water-assisted proton transfer, the calculated energy barrier, 3.2 kcal/mol, associated with transition state TS2dW-Re is 4.4 kcal/mol lower than the first step. It follows that the direct participation of the solvent water molecule in the proton transfer process decreases the energy barrier by 9.2 kcal/mol. This is why the energy barrier for the second step of the hydrolysis involving the water-assisted proton transfer is significantly lower, whereas the energy barrier for the second step involving the direct proton transfer is significantly higher than the first step. Thus, the reaction pathway involving the water-assisted proton transfer should dominate the hydrolysis in aqueous solution. Similar results were also reported for the second step of the methyl acetate hydrolysis [47].

For the second step of the cocaine methyl ester hydrolysis involving the water-assisted proton transfer, the calculated energy barrier, 4.8 kcal/mol, associated with transition state TS2dW-Me, is also lower than the corresponding first step. So, with the direct participation of the solvent water molecule in the proton transfer process, the first step of the hydrolysis in aqueous solution should be rate-determining, whether for the cocaine benzoyl ester hydrolysis or for the cocaine methyl ester hydrolysis. This conclusion provides theoretical support for the design of analogs of the first transition state for the cocaine benzoyl ester hydrolysis to elicit anti-cocaine catalytic antibodies [22, 25].

2.2
Hydrolysis of Protonated Cocaine

Under physiological conditions (pH 7.4), cocaine (pK_a 8.6) exists mainly as the protonated amine. The reaction pathways discussed above for the ester hydrolysis of neutral cocaine predict similar rates of reaction for methyl ester

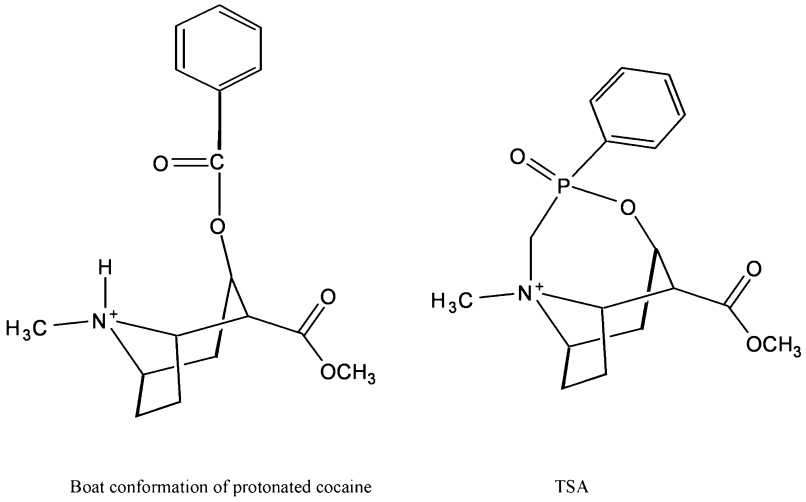

Fig. 4 Boat conformation of protonated (–)-cocaine and the corresponding TSA structure [89]

hydrolysis and benzoyl ester hydrolysis. However, the methyl ester rapidly hydrolyzes in vivo and in aqueous solution at neutral pH. Experimental kinetic studies [45] suggested that internal participation of the protonated amine in the alkaline hydrolysis of the cocaine methyl ester could account for its lability relative to the benzoyl ester.

Further, for antibody catalysis the methyl ester is too small to be an effective epitope but the participation could be induced if an antibody were able to recruit cocaine from the chair conformation to the less stable boat form (see Fig. 4 for the structure) and reorient the syn-protonated amine and benzoyl ester into proximity. Antibodies can provide significant binding energy and in principle antibody binding could effect conformer selection and promotion of substrate-assisted catalysis. To examine this idea, a detailed computational analysis [89] of the energetics of this reaction was also performed for design of novel TSA structures for the alkaline hydrolysis of boat cocaine in comparison with the hydrolysis of chair cocaine.

2.2.1 Reaction Pathways for Chair Cocaine

The first-principles reaction coordinate calculations at the B3LYP/6-31+G(d) level led to the optimized geometries of the rate-determining transition states (i.e., the transition states for the first reaction step of the ester hydrolysis), as depicted in Fig. 5. For benzoyl ester hydrolysis of protonated cocaine in its chair conformation, the nucleophilic hydroxide ion can also approach from two faces, denoted by Si and Re, of the carbonyl to form two stereoisomer

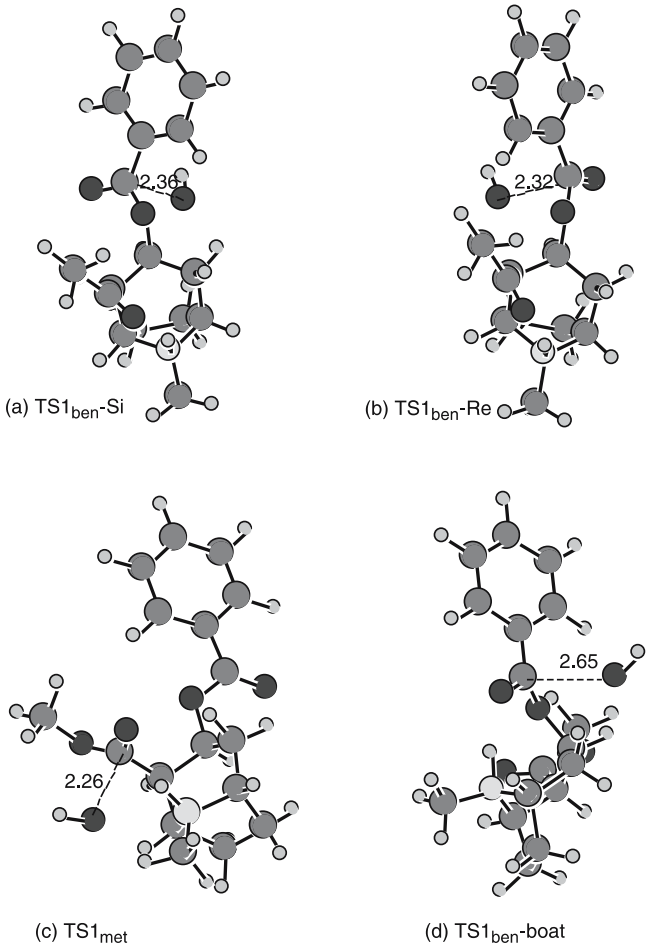

Fig. 5 Transition state structures optimized at the B3LYP/6-31+G(d) level for the ester hydrolysis of protonated cocaine [89]: **a** and **b** for the benzoyl ester hydrolysis of the chair cocaine; **c** for the methyl ester hydrolysis of the chair cocaine; and **d** for the benzoyl ester hydrolysis of the boat cocaine

tetrahedral intermediates (*R* and *S*). The two transition state structures, optimized at the B3LYP/6-31+G(d) level for the two competing pathways of the first step of the benzoyl ester hydrolysis, are denoted by $TS1_{ben}$ – Si and $TS1_{ben}$ – Re. The transition state for the first step of the cocaine methyl ester hydrolysis is denoted by $TS1_{met}$. These three transition state structures optimized for the hydrolysis of protonated cocaine are similar to the corresponding transition state structures optimized for the alkaline hydrolysis of neutral cocaine. A remarkable difference is that the internuclear distances between the hydroxide oxygen and the carbonyl carbon become significantly

shorter for the protonated cocaine: 2.36 Å, 2.32 Å, and 2.26 Å in $TS1_{ben}$ – Si, $TS1_{ben}$ – Re, and $TS1_{met}$, respectively, for protonated cocaine hydrolysis compared to the corresponding distances 2.62 Å, 2.57 Å, and 3.15 Å for neutral cocaine. These results verify earlier predictions [57, 58] made using SM3 semiempirical methods, where PM3 geometry optimizations in aqueous solution resulted in internuclear hydroxide oxygen-carbonyl carbon distances of 2.23 Å for $TS1_{ben}$ – Si and 2.13 Å for $TS1_{ben}$ – Re.

The calculated energetic results are summarized in Table 2. It should be pointed out that the ΔG(gas) values listed in Table 2 are simply the Gibbs free energy changes from the separated reactants to the corresponding transition states when the solvent effects are ignored, but these values are not the free energy barriers for the corresponding reactions in the gas phase. This is because previous studies [46–48] have demonstrated that for the reaction of an ester, the ester and hydroxide ion first form a hydrogen-bonded complex in the gas phase (a local minimum on the potential energy surface) before going to the transition state, whereas such a hydrogen-bonded complex does not exist in aqueous solution. So, the free energy barrier for the imaginary reaction in the gas phase should be the free energy change from the hydrogen-bonded complex to the first transition state.

Table 2 Calculated Gibbs free energies (in kcal/mol) of the transition states relative to the corresponding separated reactants for the ester hydrolyses of protonated cocaine in solution [89] [a]

Transition state	ΔG(gas) [b]	Solvent shift [c] Electrostatic (SVPE)	Non-electrostatic (PCM) [d]	ΔG(solution) [e] Without non-electrostatic	With non-electrostatic
$TS1_{ben}$ – Si	– 82.7	101.8	0.5	19.1	19.6
$TS1_{ben}$ – Re	– 85.3	102.1	0.1	16.8	16.9
$TS1_{met}$	– 100.4	112.9	– 1.4	12.5	11.1
$TS1_{ben}$-boat	– 81.7	98.3	0.2	16.6	16.8

ΔG is given in kcal/mol, at T = 298.15 K and P = 1 atm [a] All calculations used geometries optimized at the B3LYP/6-31+G(d) level in gas phase. The reactants are hydroxide ion and the protonated cocaine in its chair or boat conformation

[b] Calculated at the MP2/6-31+G(d)//B3LYP/6-31+G(d) level in gas phase, including zero-point vibration and thermal corrections

[c] The electrostatic part of the solvent shift was determined by performing the SVPE calculations at the HF/6-31+G(d) level, whereas the non-electrostatic contribution was determined by the PCM calculation

[d] Total contribution of short-range non-electrostatic solute-solvent interactions

[e] Gibbs free energy barrier in aqueous solution calculated as the ΔG(gas) value plus the electrostatic solvent shift determined by the SVPE calculation, without or with the non-electrostatic contributions determined by the PCM calculation

As seen in Table 2, the solvent effects are crucial for calculating realistic free energy barriers and, not surprisingly, the calculated solvent shifts are dominated by the solute–solvent electrostatic interactions. The estimated short-range non-electrostatic contributions to the free energy barriers are negligible compared to the electrostatic contributions to the solvent shifts.

The calculated free energy barriers (at $T = 298.15$ K and $P = 1$ atm) associated with transition states $TS1_{ben}$ – Si and $TS1_{ben}$ – Re for the benzoyl ester hydrolysis of protonated cocaine are 19.1 and 16.8 kcal/mol, respectively. Thus, the reaction pathway for hydroxide oxygen attacking from the Re face of the carbonyl should be dominant, which is consistent with the conclusion obtained from the energy barriers calculated for neutral cocaine hydrolysis. This is not surprising because the proton attached to the tropane N atom does not participate in the benzoyl ester hydrolysis of chair cocaine. So, the effects of the cocaine protonation on the energy barriers for the benzoyl ester hydrolysis of chair cocaine should be insignificant. Similar computations [63] on neutral cocaine hydrolysis predicted the energy barriers (i.e., the free energy barriers at $T = 0$ K) to be 8.5 and 7.6 kcal/mol, corresponding to the transition states $TS1_{ben}$ – Si and $TS1_{ben}$ – Re, respectively. The corresponding free energy barriers calculated at $T = 0$ K for the benzoyl ester hydrolysis of protonated cocaine are 9.9 and 7.0 kcal/mol. These two values become 19.1 and 16.8 kcal/mol, respectively, at $T = 298.15$ K and $P = 1$ atm. The differences between the calculated free energy barriers at $T = 0$ K and the corresponding free energy barriers at $T = 298.15$ K are primarily attributed to entropic effects, particularly the translational entropy changes from the separated reactants to the transition states.

However, the free energy barrier calculated for the methyl ester hydrolysis of protonated cocaine (2.5 kcal/mol at $T = 0$ K and 12.5 kcal/mol at $T = 298.15$ K and $P = 1$ atm) is significantly lower than that for the dominant pathway of the benzoyl ester hydrolysis (7.0 kcal/mol at $T = 0$ K and 16.8 kcal/mol at $T = 298.15$ K and $P = 1$ atm). It is also significantly lower than that for the methyl ester hydrolysis of neutral cocaine (7.0 kcal/mol at $T =$ 0 K) [63]. The significant decrease of the free energy barrier, ~ 4 kcal/mol, can be attributed to the intramolecular acid catalysis of alkaline hydrolysis of the cocaine methyl ester. This catalysis results from the interplay between two opposing factors. First, the carbonyl oxygen of the methyl ester moiety hydrogen-bonds to the tropane N through the proton at the N atom in the transition state ($TS1_{met}$) and the corresponding reactant (cocaine). The optimized internuclear distance between the carbonyl oxygen of the methyl ester moiety and the hydrogen on the tropane N is 1.801 Å in the reactant and 1.932 Å in the transition state. This NH·····O distance slightly increases in going from the reactant to the transition state, as the hydroxide oxygen gradually approaches the carbonyl carbon to form a tetrahedral intermediate. On the other hand, during the conversion of reactants to transition

state $TS1_{met}$, the partial negative charge at the carbonyl oxygen becomes progressively larger. According to the natural population analysis (NPA) [89] at the B3LYP/6-31+G(d) level, the net atomic charge at the carbonyl oxygen of the methyl ester moiety is – 0.649 in the reactant and – 0.703 in the transition state. So, there are two opposite factors affecting the change of the NH·····O hydrogen bond strength in going from the reactant to the transition state: one is the increase of the bond distance, and the other is the increase of the negative charge on the oxygen atom when the changes of the charges on the N and H atoms are negligible. The aforementioned decrease ($\sim$ 4 kcal/mol) in the free energy barrier implies that the increase of the negative charge on the oxygen atom is predominant, making the NH·····O hydrogen bonding slightly stronger in the transition state. The stronger intramolecular hydrogen bonding should contribute more effectively to TS stabilization, which explains the decrease in the free energy barrier. Furthermore, for ester hydrolysis of neutral cocaine (without a proton at the tropane N atom), the energy barrier calculated for the methyl ester hydrolysis of neutral cocaine is almost the same as that for the dominant pathway of the benzoyl ester hydrolysis [63]. With the tropane N atom being protonated, the proton is involved in the bond formation and breaking process such that the barrier becomes $\sim$ 4 kcal/mol lower for the methyl ester hydrolysis of protonated cocaine. The calculated relative magnitudes of the free energy barriers for the hydrolysis of the protonated cocaine are qualitatively consistent with the recently reported experimental results [45] of the investigations on the hydrolysis kinetics of cocaine under physiological conditions, because the cocaine methyl ester hydrolysis was found to be faster than the cocaine benzoyl ester hydrolysis.

2.2.2 Reaction Pathway for Boat Cocaine

The transition state structure, denoted by $TS1_{ben}$-boat, optimized at the B3LYP/6-31+G(d) level for the benzoyl ester hydrolysis of boat cocaine is also depicted in Fig. 5. Because the carbonyl oxygen of the benzoyl ester moiety also hydrogen-bonds to the tropane N atom through the proton at the N for boat cocaine, one might also expect similar intramolecular acid catalysis of the benzoyl ester hydrolysis of boat cocaine as seen in the methyl ester hydrolysis of chair cocaine discussed above. The free energy barrier (7.2 kcal/mol at $T = 0$ K and 16.6 kcal/mol at $T = 298.15$ K and $P = 1$ atm) calculated for the benzoyl ester hydrolysis of boat cocaine is significantly higher than that for the methyl ester hydrolysis of chair cocaine and, at $T = 298.15$ K and $P = 1$ atm, is only 0.2 kcal/mol lower than that for the dominant pathway of the benzoyl ester hydrolysis of chair cocaine. This is because the optimized distance between the carbonyl oxygen of the benzoyl ester moiety and the hydrogen on the tropane N significantly increases from 1.632 Å in the

reactant (boat cocaine) to 2.027 Å in the transition state $TS1_{ben}$-boat while the net negative charge (NPA charge) at the carbonyl oxygen of the benzoyl ester moiety increases slightly from – 0.657 in the reactant to – 0.670 in the transition state. Note that the atomic charges determined by NPA or any other theoretical approach may only be used to qualitatively assess the change of the charge, as the absolute charges calculated are closely dependent on the theoretical approach used in the calculation. Qualitatively, the calculated increase of the negative charge from the reactant to the transition state for the benzoyl ester hydrolysis of the boat cocaine is smaller than that calculated for the methyl ester hydrolysis of chair cocaine, implying that the factor of the charge increase for the benzoyl ester hydrolysis of the boat cocaine is less significant than that for the methyl ester hydrolysis of chair cocaine. Overall, the effects of the two opposite factors (i.e., the increase of the NH·····O distance and increase of the negative charge on the O atom) on the free energy barrier nearly cancel out for the methyl ester hydrolysis of chair cocaine. Alternatively, one can describe the intramolecular catalysis of boat cocaine as a process that overcomes the unfavorable steric interactions produced by crowding when the more favorable chair conformation converts to the boat conformation. Intramolecular catalysis of this more crowded species has roughly the same free energy of activation as does regular intermolecular catalysis of the benzoyl ester.

Of greater interest is that the free energy barrier for the benzoyl ester hydrolysis of boat cocaine is not higher than for the benzoyl ester hydrolysis of chair cocaine [89]. This result implies that a TSA structure (Fig. 4) for intramolecular hydrolysis might yield catalysts that would recruit a functional group from the substrate. Thus these theoretical calculations answer a global question: Is the benzoyl ester hydrolysis of boat cocaine even plausible? The similar free energy barriers calculated for the benzoyl ester hydrolysis of the chair and boat cocaine structures support this concept. Intramolecular hydrogen bonding could be useful in generating antibody-based catalysts that recruit cocaine to the boat conformation, and an analog that elicited antibodies to approximate the protonated tropane N and the benzoyl O more closely than the natural boat conformer might increase the contribution from hydrogen bonding.

2.2.3
Development of Anti-cocaine Catalytic Antibodies

The first anti-cocaine catalytic antibody was reported by Landry and associates in 1993 [22]. The transition-state analog used to elicit the first anti-cocaine catalytic antibody was a stable structure of the transition state for the benzoyl ester hydrolysis of chair cocaine [22, 25]. Based on the computational analysis discussed above, the new TSA structure depicted in Fig. 4 was synthesized and 85 cocaine esterases out of 450 anti-analog antibodies

were elicited [94] – a performance markedly superior to that of a previously employed simple phosphonate ester as a stable analog of the transition state structure for the benzoyl ester hydrolysis of chair cocaine [22, 25, 95]. In turn, the encouraging experimental results [94] support the thrust of the computational studies [89]. (As noted in [89] the computational studies described in [89], published in 2005, were actually completed far before the experimental studies described in 2004 in [94], but publication had been considerably delayed.)

3
Mechanism for BChE-Catalyzed Hydrolysis of Cocaine

3.1
3D Structure of BChE

To uncover the detailed reaction pathway for BChE-catalyzed hydrolysis of a substrate, one first needs to know the 3D structure of the enzyme. The first X-ray crystal structure of BChE was reported in later 2003 [96]. However, some computational studies on BChE–cocaine binding and on the fundamental reaction pathway were reported in literature prior to the report of the first X-ray crystal structure of BChE. The computational studies [97–100] reported prior to the report of the X-ray crystal structure were based on a homology model of BChE constructed from the solved X-ray crystal structure of *Torpedo californica* acetylcholinesterase (AChE). A detailed comparison [101] of the X-ray crystal structure with the homology model of BChE reveals that the overall structure of the homology model is very close to that of the X-ray crystal structure; the only significant difference can be seen at the acyl binding pocket. The similarity between the X-ray crystal structure and homology model of BChE, along with further computational modeling using the X-ray crystal structure, confirms the fundamental structural and mechanistic insights [100] obtained from the computational studies based on the homology model.

3.2
Fundamental Reaction Pathways

3.2.1
Similarity between Structures of Cocaine and Butyrylcholine

Reaction coordinate calculations for a chemical reaction begin with a concept of the orientation of the reactants. Different starting structures for the enzyme–substrate complex can lead to completely different reactions. For such enzymatic reactions, one needs to know the structure of the prereactive

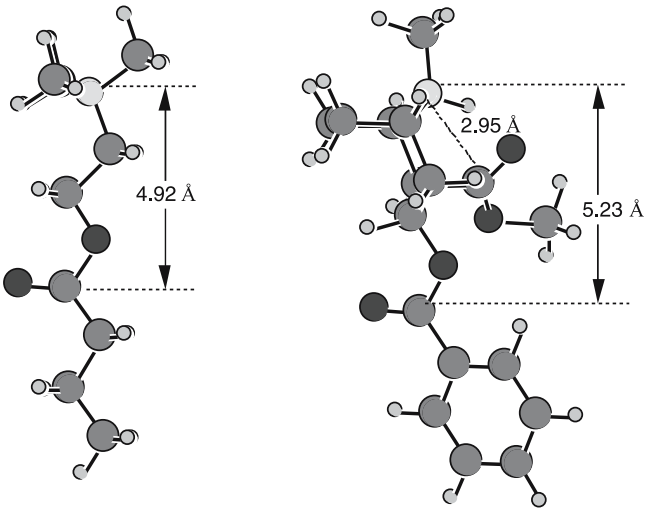

Fig. 6 Geometries of BCh and (–)-cocaine optimized at the B3LYP/6-31+G(d) level [100]

enzyme–substrate complex, which may also be called the "near attack conformation" (NAC) defined by Bruice et al. [102] and discussed more carefully by Shurki et al. [103]. The initial insights into the enzyme–substrate binding came from a comparison of the optimized geometry of butyrylcholine (BCh) with those of (–)-cocaine and (+)-cocaine [100].

The geometries of BCh and (–)-cocaine optimized at the B3LYP/6-31+G(d) level are depicted in Fig. 6. Note that cocaine mainly exists in its protonated form under physiological condition because its pK_a is 8.6 [45], and thus both BCh and cocaine have positively charged quaternary ammonium groups. In human BChE, W82 is thought to be the key factor in the stabilization of positively charged substrates in the BChE-substrate complexes, although this interaction should be more properly classified as a cation-π interaction [104]. While the positively charged quaternary ammonium is positioned to effectively bind with W82 in the prereactive BChE-substrate complex, the carbonyl carbon of the substrate must be positioned proximal to S198 O^{γ} for nucleophilic attack. Thus the distance between the carbonyl carbon and the quaternary ammonium is critical and according to the optimized geometries depicted in Fig. 6, this distance is 4.92 Å for the excellent substrate BCh. The optimized C to N distance for the substrate cocaine benzoyl ester (5.23 Å) is similar to that of BCh. The C to N distance for the cocaine methyl ester (2.95 Å) is remarkably shorter. This helps to explain why (–)-cocaine and (+)-cocaine bind with BChE in such a way as to hydrolyze at the benzoyl ester, instead of at the methyl ester. In contrast, for the non-enzymatic hydrolysis of cocaine under physiological conditions (pH 7.4, 37 °C) the methyl ester hydrolyzes faster than the benzoyl [45].

3.2.2 BChE–Substrate Complexes

Based on the structural similarity discussed above, the relative positions of the positively charged quaternary ammonium and the carbonyl group of the benzoyl ester moiety in the prereactive BChE–cocaine complexes could be similar to those in the corresponding BChE–BCh complex. The main structural difference between the BChE-(–)-cocaine and BChE-(+)-cocaine complexes exists only in the relative position of the methyl ester group (Fig. 1). Hence, the initial structures of both the BChE-(–)-cocaine and BChE-(+)-cocaine complexes used in molecular modeling and simulations were generated from a 3D model of human BChE with substrate butyrylcholine (BCh), constructed by Harel et al. [105, 106] by replacement of substrate. (–)-Cocaine and (+)-cocaine were positioned similarly to BCh: the carbonyl group of the benzoyl ester was superimposed on the carbonyl group of BCh, and the nitrogen at the positively charged tropane nucleus was superimposed on the nitrogen of the positively charged quaternary ammonium.

The energy-minimized geometries of the BChE-(–)-cocaine and BChE-(+)-cocaine complexes are depicted in Fig. 7a and b, showing the interactions of the carbonyl group of the benzoyl ester with the hydroxyl oxygen (O^{γ}) of S198 and with the oxyanion hole formed by the peptidic NH functions of G116, G117, and A199. In the minimized structures of BChE binding with (–)-cocaine and (+)-cocaine, the internuclear distances between the carbonyl carbon of the benzoyl ester and S198 O^{γ} are 3.19 and 3.18 Å, respectively. During the MD simulations from 100 ps to 500 ps, the time-average values of the distance between the carbonyl carbon and S198 O^{γ} are $\sim$ 3.51 and $\sim$ 3.53 Å for (–)-cocaine and (+)-cocaine, respectively [100]. These C to O^{γ} distances are all comparable to the distances between the carbonyl carbon and the hydroxide oxygen (2.99–3.56 Å) [46] in the optimized geometries of the prereactive complexes of carboxylic acid esters with hydroxide ion [46–48]. The distances between the carbonyl oxygen of the benzoyl ester and the NH hydrogen of G116, G117, and A199 are 1.98, 2.59, and 1.92 Å, respectively, in the minimized structures of BChE with (–)-cocaine. The respective O to H distances in the minimized structures of BChE with (+)-cocaine are 1.82, 2.42, and 2.39 Å. The respective time-average values of the O to H distances are $\sim$ 3.67, $\sim$ 2.21, and $\sim$ 2.46 Å for the MD simulation on BChE with (–)-cocaine, and $\sim$ 3.80, $\sim$ 2.39, and $\sim$ 3.01 Å for the MD simulation with (+)-cocaine [100]. In addition, the MD trajectories also reveal that in both the BChE-(–)-cocaine and BChE-(+)-cocaine complexes, the cocaine nitrogen atom stays at nearly the same position as the BCh nitrogen atom in the structure of the BChE model constructed by Harel et al. [106]. These limited results suggest that both (–)-cocaine and (+)-cocaine may bind with human BChE so as to allow S198 O^{γ} to approach the carbonyl carbon of the benzoyl ester.

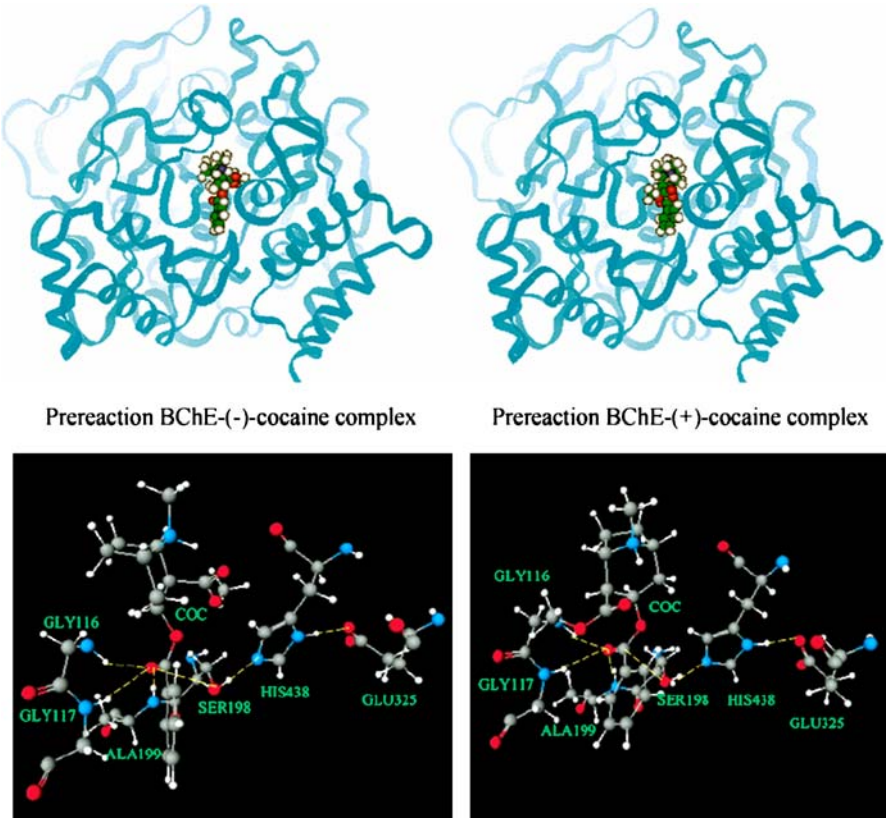

Fig. 7 Minimized structures of prereactive BChE-(–)-cocaine and BChE-(+)-cocaine complexes [100]: **a** ribbon; **b** residues forming the catalytic triad and the three-pronged oxyanion hole

The energy-minimized structures of the prereactive BChE-(–)-cocaine and BChE-(+)-cocaine complexes depicted in Fig. 7 are similar to the prereactice enzyme–substrate structure proposed for BChE binding with other positively charged substrates, i.e., butyrylthiocholine and succinyldithiocholine [104, 107]; they are all positioned horizontally at the bottom of the substrate-binding gorge of BChE. To better understand BChE binding with cocaine, (–)-cocaine and (+)-cocaine were also docked to the BChE active site in order to model the non-prereactive enzyme–substrate complexes. In the MD-simulated non-prereactive BChE-(–)-cocaine and BChE-(+)-cocaine complexes, (–)-cocaine and (+)-cocaine are positioned vertically in the substrate-binding gorge between D70 and W82. The MD trajectories for the non-prereactive BChE-(–)-cocaine and BChE-(+)-cocaine complexes are also very stable. In addition, the simulated non-prereactive BChE-(–)-cocaine and BChE-(+)-cocaine complexes are very close to the simulated

Michaelis–Menten complexes reported by Sun et al. [97]. All these suggest that the binding of BChE with (–)-cocaine and (+)-cocaine is similar to those proposed with butyrylthiocholine and succinyldithiocholine. Both the non-prereactive and prereactive enzyme–substrate complexes could exist before going to the chemical reaction steps.

To better compare the modeled non-prereactive complex with the prereactive complex for (–)-cocaine and for (+)-cocaine, the protein backbone atoms in the non-prereactive complex were superimposed with the corresponding atoms in the prereactive complex [100]. It turns out that the overall protein structures in the non-prereactive and prereactive complexes are very close to each other, while the orientations of the substrate are nearly vertical to each other. So, for both (–)-cocaine and (+)-cocaine, the substrate needs to rotate about 90° [100] during the change from the non-prereactive complex to the prereactive complex; more specifically, (–)-cocaine needs to rotate slightly more than (+)-cocaine. The energy barrier of the change from the non-prereactive complex to the prereactive complex for (–)-cocaine is expected to differ from that for (+)-cocaine. This is because the relative positions of the C-2 methyl ester group of substrate are different and, therefore, some amino acid residues hindering the rotation of one substrate might not hinder the rotation of another. Specific residues possibly hindering substrate rotation will be discussed below.

It is apparent that a detailed mechanistic understanding of the difference between the catalytic activity of BChE for (+)-cocaine and for (–)-cocaine could lead to important insights for the rational design of esterases with a high catalytic activity for hydrolysis of natural (–)-cocaine.

3.2.3 Possible Reaction Pathways

For both (–)-cocaine and (+)-cocaine, the relative positions of the nitrogen and the benzoyl carbonyl in the simulated prereactive BChE-substrate complex are essentially the same as those reported for BCh in BChE [100]. One may expect that BChE-catalyzed hydrolysis of (–)-cocaine and (+)-cocaine follow a reaction pathway similar to that for BChE-catalyzed hydrolysis of BCh. A remarkable difference between (–)-cocaine and (+)-cocaine is associated with the relative positions of the C-2 methyl ester group. The C-2 methyl ester group of (–)-cocaine remains on the same side of the carbonyl of the benzoyl ester as the attacking hydroxyl oxygen (S198 O^{γ}), whereas the C-2 methyl ester of (+)-cocaine remains on the opposite side. This difference could cause a difference in hydrogen bonding, electrostatic, and van der Waals interactions during the catalytic process, and result in a significant difference in free energies of activation. Nevertheless, the basic BChE mechanism for both enantiomers may resemble the common catalytic mechanism for ester hydrolysis in other serine hydrolases [100, 108], including

the thoroughly investigated AChE [109–112]. Thus, based on the modeling and simulation of the prereactive complexes and the knowledge about ester hydrolysis in other serine hydrolases, a possible reaction pathway for BChE-catalyzed hydrolysis of cocaine can be hypothesized. Scheme 1 depicts

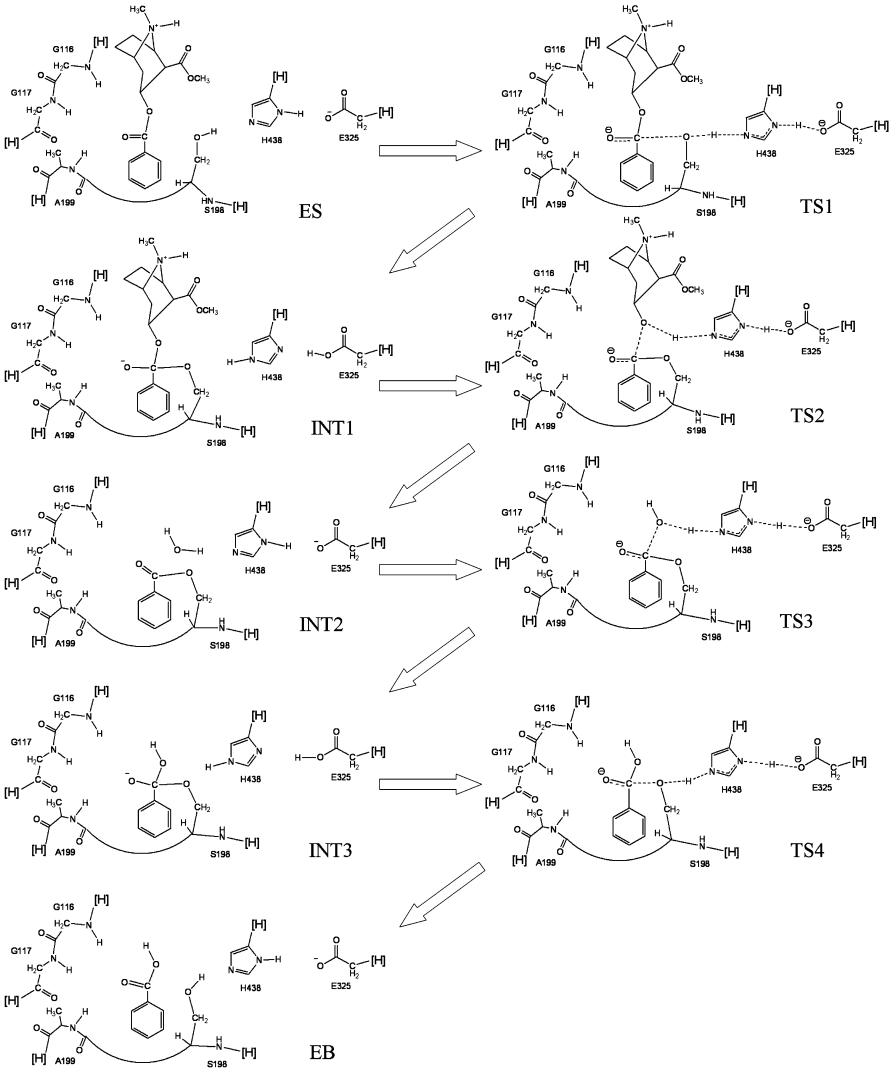

Scheme 1 Schematic representation of BChE-catalyzed hydrolysis of (–)-cocaine. Only the QM-treated high-layer part of the reaction system in the ONIOM (QM/MM) calculations [113] are drawn. Notation [H] refers to a non-hydrogen atom in the MM-treated low-layer part of the protein, and the cut covalent bond with this atom is saturated by a hydrogen atom. The transition covalent bonds existing in all of the transition states are indicated with *dashed lines*

(–)-cocaine and important groups from the catalytic triad (S198, E325, and H438) and three-pronged oxyanion hole (G116, G117, and A199). The proposed hydrolysis of cocaine consists of both the acylation and deacylation stages demonstrated for ester hydrolysis by other serine hydrolases. A significant difference might exist in the number of potential hydrogen bonds involving the carbonyl oxygen in the oxyanion hole. The three-pronged oxyanion hole formed by peptidic NH groups of G116, G117, and A199 in BChE (or by peptidic NH groups of G118, G119, and A201 in AChE) contrasts with the two-pronged oxyanion hole of many other serine hydrolases. Schematic representation of the pathway for (+)-cocaine hydrolysis should be similar to Scheme 1, differing only in the relative position of the C-2 methyl ester group in the acylation.

As depicted in Scheme 1 [113], the acylation is initialized by S198 O^{γ} attack at the carbonyl carbon of the cocaine benzoyl ester to form the first tetrahedral intermediate (INT1) through the first transition state (TS1). During the formation of INT1, the C – O bond between the carbonyl carbon and S198 O^{γ} gradually forms, while the proton at S198 O^{γ} gradually transfers to the imidazole N atom of H438, which acts as a general base. The second step of the acylation is the decomposition of INT1 to the metabolite ecgonine methyl ester and acyl-BChE (INT2a) through the second transition state (TS2). During the change from INT1 to INT2a, the proton gradually transfers to the benzoyl ester oxygen, while the C – O bond between the carbonyl carbon and the ester oxygen gradually breaks. Also, during the first step of acylation, the carbonyl oxygen may potentially form up to three hydrogen bonds with the NH groups of G116, G117, and A199.

In the MD-simulated prereactive enzyme–substrate complex [100], only one or two of the three NH groups weakly hydrogen-bond to the carbonyl oxygen of (+)-cocaine or (–)-cocaine during the simulations. No hydrogen bonding was noted between the carbonyl oxygen and the NH group of G116. These potential hydrogen bonds are expected to increase in strength from ES to TS1 and to INT1 due to the expected increase of net negative charge on the carbonyl oxygen. By the same logic, these potential hydrogen bonds are expected to progressively weaken from INT1 to TS2 and to INT2. The deacylation is initialized by water (oxygen) attack at the carbonyl carbon with participation of H438 as a general base, and is the reverse of acylation with respect to bond breaking/formation and potential hydrogen bonds.

3.2.4
Reaction Coordinates and Energy Barriers

To examine the above mechanistic hypotheses, detailed first-principles reaction coordinate calculations [100] were performed on the fundamental reaction pathways for BChE-catalyzed hydrolysis of (–)-cocaine with a BChE active site model. The BChE active site model used in the reaction coordi-

nate calculations includes only the six amino acids indicated in Scheme 1 with the following simplifications: S198 is represented by methanol, H438 is represented by imidazole, E325 is represented by acetate (CH_3COO^-), and G116, G117, and A199 are all represented by ammonia molecules. This BChE active site model consists of 34 atoms. So, a total of 78 atoms were included in the ab initio calculations [100] on the model of (–)-cocaine hydrolysis. Reaction coordinate calculations on this model system are expected to provide a qualitative picture for the formation and breaking of covalent bonds at the reaction center and to estimate the intrinsic energy barriers and Gibbs free energy barriers for the enzymatic reaction.

The reaction coordinate calculations [100] confirmed the mechanistic hypothesis depicted in Scheme 1, i.e., the entire chemical reaction process consists of four individual steps (ES → TS1→ INT1 → TS2 → INT2 → TS3 → INT3 → TS4 → EB). The calculated energy barriers (ΔE_a) and Gibbs free energy barriers (ΔG_a) are summarized in Table 3.

Similar computational studies [46–48] on the reaction pathways for various non-enzymatic ester hydrolyses demonstrate that electron correlation effects are important only for final energy evaluations, but are not important for the geometry optimizations. The geometry optimizations at a lower HF level (using a smaller basis set) followed by single-point energy calculations at the MP2/6-31+G(d) level are adequate for predicting energy barriers in excellent agreement with the corresponding experimental data. The calculations at higher levels, e.g., replacing MP2 with QCISD(T) or using larger basis set, do not change the calculated energy barriers substantially [46, 47]. As seen in Table 3, the results calculated at the MP2/6-31+G(d)//HF/3-21G level show that for both the acylation and deacylation stages, the energy bar-

Table 3 Energy barriers (ΔE_a) and Gibbs free energy barriers (ΔG_a), in kcal/mol, calculated for BChE-catalyzed hydrolysis of (–)-cocaine at 298 K and 1 atm [100] [a]

Method	ΔE_a				ΔG_a			
	Step 1	Step 2	Step 3	Step 4	Step 1	Step 2	Step 3	Step 4
MP2/6-31+G(d)	4.0	3.1	16.6 (17.0)	6.5	5.6	3.6	19.0 (18.2)	6.6
B3LYP/6-31+G(d)	6.2		16.9 (18.5)		7.8		19.2 (19.8)	
B3LYP/6-31+G(d,p)	5.5		16.2 (17.5)		7.1		18.5 (18.7)	
B3LYP/6-31++G(d,P)	5.6		16.2 (17.5)		7.2		18.5 (18.7)	

[a] Values in parentheses were calculated using the geometries optimized at the B3LYP/6-31G(d) level. Other values were calculated using the geometries optimized at the HF/3-21G level

rier and free energy barrier predicted for the first step (i.e., the first or third step of the entire chemical reaction process) is always higher than that for the corresponding second step (i.e., the second or fourth step of the entire chemical reaction process). Hence, the B3LYP energy calculations using the 6-31+G(d) and larger basis sets were also performed on these two critical reaction steps. The energy barriers calculated at the B3LYP/6-31+G(d) level are close to the corresponding values at the MP2/6-31+G(d) level. Increasing the basis set from 6-31+G(d) to 6-31++G(d,p), the changes of the calculated barriers are smaller than 0.7 kcal/mol.

Since the third reaction step (i.e., the first step of deacylation) is associated with the highest energy barrier and the highest Gibbs free energy barrier, the geometries of TS3 and INT2 were also optimized at the B3LYP/6-31G(d) level to evaluate the barrier for this highest-barrier reaction step using the B3LYP/6-31G(d) geometries. It has been found that the barriers calculated using the B3LYP/6-31G(d) geometries are close to those from the HF/3-21G geometries, particularly for the Gibbs free energy barriers. These comparisons indicate that the energy barriers and Gibbs free energy barriers predicted at the MP2/6-31+G(d)//B3LYP/6-31G(d) and MP2/6-31+G(d)//HF/3-21G levels are reliable.

Because the third reaction step is predicted to have the highest barrier, this reaction step is expected to be rate determining if the effects of the remaining protein environment on the calculated barriers can be neglected. Further, because the third reaction steps for (–)-cocaine and for (+)-cocaine are identical, their hydrolysis rates in BChE would be expected to be the same if this step of the chemical reaction process were really rate determining for the entire catalytic process. In fact, (–)-cocaine hydrolysis in BChE is about 1000 to 2000 times slower than (+)-cocaine, suggesting that some other factors, such as the change from the non-prereactive complex to the prereactive complex (ES), are important for (–)-cocaine or for both (–)-cocaine and (+)-cocaine. Furthermore, if a chemical reaction step in the acylation, rather than the transformation from non-prereactive BChE-(–)-cocaine complex to the prereactive BChE-(–)-cocaine complex, is rate determining, the enzymatic reaction rate is expected to be pH-dependent. An experimental study [97] revealed that the rate of the BChE-catalyzed hydrolysis of (–)-cocaine is not significantly affected by the pH of the reaction solution, whereas the rate of the BChE-catalyzed hydrolysis of (+)-cocaine is clearly pH-dependent. So, it is likely that the rate-determining step is the change from the non-prereactive complex to the prereactive complex for BChE-catalyzed hydrolysis of (–)-cocaine [100].

3.3 MD Simulations of Cocaine Binding with BChE Mutants

The enzyme–substrate binding and fundamental reaction pathways discussed above provide a rational base for the design of more active BChE

mutants for catalytic hydrolysis of (–)-cocaine. Now that the change from the non-prereactive complex to the prereactive complex is probably the rate-determining step of the BChE-catalyzed hydrolysis of (–)-cocaine, useful BChE mutants could be designed to specifically accelerate the change from the non-prereactive BChE-(–)-cocaine complex to the prereactive BChE-(–)-cocaine complex. A detailed analysis of the MD-simulated structures of wild-type BChE binding with (–)-cocaine and (+)-cocaine revealed that Y332 is a key residue hindering the structural change from the non-prereactive BChE-(–)-cocaine complex to the prereactive BChE-(–)-cocaine complex [100, 101]. A number of possible mutants of BChE were proposed for wet experimental tests [97–101, 114]. The earliest design of BChE mutants was only based on the modeled or simulated structure of the non-prereactive BChE-(–)-cocaine complex with wild-type BChE; the possible dynamics of the proposed BChE mutants were not examined. Some of the proposed mutants indeed have an improved catalytic efficiency against (–)-cocaine [97–99, 101, 114].

In order to more reliably predict the BChE mutants with a possibly higher catalytic efficiency against (–)-cocaine, MD simulations were also performed on the structures of (–)-cocaine binding with a number of hypothetical BChE mutants in their non-prereactive and prereactive complexes [101]. Table 4 summarizes the average values of some important geometric parameters in the simulated complexes.

In the simulated non-prereactive complex, the average distance between the carbonyl carbon of cocaine benzoyl ester and S198 O^{γ} is 7.6 Å for A328W/Y332A BChE and 7.1 Å for A328W/Y332G BChE, as seen in Table 4. In the simulated prereactive complex, the average values of this important internuclear distance become 3.87 and 3.96 Å for A328W/Y332A and A328W/Y332G BChEs, respectively. Compared to the simulated wild-type BChE-(–)-cocaine prereactive complex, the average distances between the carbonyl carbon of the cocaine benzoyl ester and S198 O^{γ} in the prereactive complex of (–)-cocaine with A328W/Y332A and A328W/Y332G BChEs are all slightly longer, whereas the average distances between the carbonyl oxygen of the cocaine benzoyl ester and the NH of G116, G117, and A199 residues are all shorter. This suggests that (–)-cocaine more strongly binds with A328W/Y332A and A328W/Y332G BChEs in the prereactive complexes. More importantly, the (–)-cocaine rotation in the active site of A328W/Y332A and A328W/Y332G BChEs from the non-prereactive complex to the prereactive complex did not cause considerable changes of the positions of A332 (or G332), W328, and F329 residues, compared to the (–)-cocaine rotation in the active site of wild-type BChE. These results suggest that A328W/Y332A and A328W/Y332G BChEs should be associated with lower energy barriers than the wild-type for the (–)-cocaine rotation from the non-prereactive complex to the prereactive complex. Further, (–)-cocaine binding with A328W/Y332G BChE is very similar to the binding with A328W/Y332A BChE, but the pos-

Table 4 Time-averaged values of some key geometric parameters (Å and degree) in the simulated non-prereactive and prereactive BChE-cocaine complexes [101]

BChE-cocaine binding[a]	Average values of the geometric parameters[c]						RMSD[d]	
	$<D1>_{non}$	<D1>	<D2>	<D3>	<D4>	$<\Theta>$	nonpre	pre
Wild-type	5.60	3.27	5.77	2.71	3.37	67	1.14	1.27
Wild-type with (+)-cocaine[b]	7.64	3.69	2.88	2.30	2.83	61	1.15	1.13
A328W/Y332A	7.11	3.87	3.30	2.14	3.01	51	1.58	1.65
A328W/Y332G	7.06	3.96	2.28	2.52	2.42	60	1.20	1.35
A328W/Y332A/Y419S	5.18	5.84	5.64	4.56	6.97	164	2.66	2.62

[a] Refers to (–)-cocaine binding with wild-type human BChE or (–)-cocaine binding with a mutant BChE, unless indicated otherwise

[b] Refers to (+)-cocaine binding with wild-type human BChE

[c] $<D1>_{non}$ and <D1> represent the average distances between the S198 O^{γ} atom and the carbonyl carbon of the cocaine benzoyl ester in the simulated non-prereactive and prereactive BChE-cocaine complexes, respectively. <D2>, <D3>, <D4> refer to the average values of the simulated distances from the carbonyl oxygen of the cocaine benzoyl ester to the NH hydrogen atoms of G116, G117, and A199 residues, respectively. $<\Theta>$ is the average value of the dihedral angle formed by the S198 O^{γ} atom and the plane of the carboxylate group of the cocaine benzoyl ester

[d] Root-mean-square deviation (RMSD) of the coordinates of backbone atoms in the simulated structure from those in the X-ray crystal structure of BChE. *nonpre* and *pre* refer to the non-prereactive and prereactive BChE-cocaine complexes, respectively

ition change of F329 residue caused by the (–)-cocaine rotation was significant only in A328W/Y332A BChE, thus suggesting that the energy barrier for the (–)-cocaine rotation in A328W/Y332G BChE should be slightly lower than that in A328W/Y332A BChE.

Concerning (–)-cocaine binding with A328W/Y332A/Y419S BChE, Y419 stays deep inside the protein and does not directly contact with the cocaine molecule. The Y419S mutation was considered because this mutation was initially expected to further increase the free space of the active site pocket so that the (–)-cocaine rotation could be easier. However, as seen in Table 4, the average distance between the carbonyl carbon of cocaine benzoyl ester and S198 O^{γ} atom in the simulated prereactive complex was as long as 5.84 Å. The average distances between the carbonyl oxygen of the cocaine benzoyl ester and the NH hydrogen atoms of G116, G117, and A199 residues are between 4.56 and 6.97 Å; no any hydrogen bond between them. In addition to the internuclear distances, another interesting geometric parameter is the dihedral angle, Θ, formed by S198 O^{γ} and the plane of the carboxylate group of the cocaine benzoyl ester. As seen in Table 4, the Θ values in the prereactive complexes of cocaine with wild-type BChE and all of the BChE mutants, other than A328W/Y332A/Y419S BChE, all slightly deviate from the

ideal value of 90° for the nucleophilic attack of S198 O^{γ} at the carbonyl carbon of cocaine. The Θ value in the prereactive complex of (–)-cocaine with A328W/Y332A/Y419S BChE is 164°, which is considerably different from the ideal value of 90°.

The above discussion suggests that the energy barriers for the (–)-cocaine rotation in A328W/Y332A and A328W/Y332G BChEs from the nonprereactive complex to the prereactive complex, the rate-determining step for the BChE-catalyzed hydrolysis of (–)-cocaine, should be lower than that in wild-type BChE. Thus, the MD simulations predict that both A328W/Y332A and A328W/Y332G BChEs should have a higher catalytic efficiency than wild-type BChE for (–)-cocaine hydrolysis. Further, the MD simulations also suggest that the energy barrier for the (–)-cocaine rotation in A328W/Y332G BChE should be slightly lower than that in A328W/Y332A BChE and, therefore, the catalytic efficiency of A328W/Y332G BChE for the (–)-cocaine hydrolysis should be slightly higher than that of A328W/Y332A BChE. In addition, the MD simulations predict that A328W/Y332A/Y419S BChE should have no catalytic activity, or have a considerably lower catalytic efficiency than the wild-type, for (–)-cocaine hydrolysis because (–)-cocaine binds with the mutant BChE in a way that is not suitable for the catalysis. Following the computational predictions, the wet experimental studies (including site-directed mutagenesis, protein expression, and enzyme activity assay against (–)-cocaine) were carried out [101]. The experimental kinetic data qualitatively confirms the theoretical predictions based on the MD simulations. In particular, the catalytic efficiency of A328W/Y332G BChE is indeed slightly higher than that of A328W/Y332A BChE against (–)-cocaine, and A328W/Y332A/Y419S BChE is indeed inactive against (–)-cocaine [101].

3.4 Evolution of Hydrogen Bonding during the Reaction Process

3.4.1 Theoretical Issue for MD Simulation of a Transition State

To examine the evolution of hydrogen bonding during the reaction process through MD simulations, one needs to perform MD simulations on all of the transition states, in addition to the routine MD simulations on the reactants, intermediates, and products. One must address a critical issue [115–118] before performing any MD simulation on a transition state. In principle, MD simulation using a classical force field (molecular mechanics) can only simulate a stable structure corresponding to a local minimum on the potential energy surface, whereas a transition state during a reaction process is always associated with a first-order saddle point on the potential energy surface. Hence, MD simulation using a classical force field cannot directly simulate a transition state without any restraint on the geometry of the transition state.

Nevertheless, if one can technically remove the freedom of imaginary vibration in the transition state structure, then the number of vibrational freedoms (normal vibration modes) for a non-linear molecule will decrease from 3N – 6 to 3N – 7 (or less). The transition state structure is associated with a local minimum on the potential energy surface within a subspace of the reduced vibrational freedoms, although it is associated with a first-order saddle point on the potential energy surface with all of the 3N – 6 vibrational freedoms. Theoretically, the vibrational freedom associated with the imaginary vibrational frequency in the transition state structure can be removed by appropriately freezing the reaction coordinate. The reaction coordinate corresponding to the imaginary vibration of the transition state is generally characterized by a combination of some key geometric parameters. These key geometric parameters are bond lengths of the forming and breaking covalent bonds for BChE-catalyzed hydrolysis of cocaine. Thus, one just needs to maintain the bond lengths of the forming and breaking covalent bonds during the MD simulation on a transition state [115–117].

Technically, one can maintain the bond lengths of the forming and breaking covalent bonds by simply fixing all atoms within the reaction center, by using some constraints on the forming and breaking covalent bonds, or by redefining the forming and breaking covalent bonds. It should be pointed out that the purpose of performing such type of MD simulation on a transition state is to examine the dynamic change of the protein environment surrounding the reaction center and the interaction between the reaction center and the protein environment. The detailed MD procedure for transition state simulation has been described in the latest literature [115–117].

3.4.2 Structures from MD Simulations and QM/MM Optimizations

All transition states and intermediates need to be simulated, allowing the protein structure to have a sufficiently long time to adapt to the fixed reaction center geometries obtained from the earliest ab initio reaction coordinate calculations [100]. The MD trajectories actually became stable quickly [115], so were the internuclear distances involved in the potential N – H···O hydrogen bonds, i.e., the distances from the carbonyl oxygen (denoted by O31) of cocaine benzoyl ester to the NH hydrogen atoms of G116, G117, and A199. The numerical results concerning the MD trajectories are summarized in Table 5. As seen in Table 5, the RMSD values are all smaller than 2.0 Å for all of the MD trajectories, demonstrating that the backbone of BChE did not dramatically change in going from the prereactive BChE–cocaine complex (ES) to the transition states, intermediates, and product.

As seen in Table 5, in the QM/MM-optimized geometries, the distances optimized for TS3 and INT3 (associated with the rate-determining step of the chemical reaction process) at the B3LYP/6-31+G(d):Amber level

Table 5 Summary of the MD-simulated and optimized key distances (Å) and the root-mean-square deviation (RMSD) of the simulated structures from the initial structure [115]

Structure	Method	Distance[a]					RMSD[b]
		D1	D2	D3	D4	D5	
ES	MD[c]	3.79	2.14	4.47	3.11	4.89	1.28
	QM/MM(a)[d]	4.05	2.16	4.60	3.41	5.22	
TS1	MD	4.59	2.91	1.92	2.00	3.61	1.59
	QM/MM(a)	4.12	2.24	2.04	2.34	4.36	
INT1	MD	3.92	1.94	2.36	2.08	4.01	1.57
	QM/MM(a)	4.09	2.03	1.93	2.06	4.04	
TS2	MD	3.49	1.98	2.22	2.26	4.13	1.53
	QM/MM(a)	3.55	1.80	1.90	2.36	4.54	
INT2	MD	3.12	2.15	2.50	3.94	3.37	1.76
	QM/MM(a)	2.60	1.89	2.81	5.15	3.41	
TS3	MD	3.76	1.98	2.68	3.86	1.96	1.61
	QM/MM(a)	3.76	2.14	1.87	4.04	2.07	
	QM/MM(b)[d]	4.10	2.27	1.85	3.99	2.07	
INT3	MD	3.01	2.03	1.88	4.05	5.68	1.70
	QM/MM(a)	2.04	1.80	1.64	4.27	6.07	
	QM/MM(b)	2.23	1.73	1.69	4.18	6.00	
TS4	MD	3.73	2.04	1.87	3.04	4.26	1.53
	QM/MM(a)	3.24	1.91	1.69	2.96	4.84	
EB	MD	4.14	3.22	4.23	3.64	2.06	1.48
	QM/MM(a)	3.37	2.14	2.12	4.87	2.87	
BChE[e]	MD				3.64	4.35	1.49
AChE-ACh[f]	MD	2.32	1.92	3.53	4.17	5.40	1.37

[a] D1, D2, and D3 represent the distances between the carbonyl oxygen of cocaine benzoyl ester and the NH hydrogen of G116, G117, and A199, respectively. D4 and D5 respectively refer to the distances between the NH hydrogen of G116 and the oxygen atoms $O^{\varepsilon 1}$ and $O^{\varepsilon 2}$ of E197 side chain

[b] Root-mean-square deviation of the coordinates of backbone atoms in the simulated structure from those in the initial structure

[c] Average distances from the stable trajectory of MD simulation

[d] Distances in the geometry optimized by performing the QM/MM calculation at the HF/3-21G:Amber level (a) or at the B3LYP/6-31+G(d):Amber level (b). The bond lengths for all of the transition bonds were fixed in the geometry optimizations

[e] Results for the pure protein without cocaine or any other ligand in the active site

[f] Results for prereactive complex between mouse acetylcholinesterase (AChE) and acetylcholine (ACh). For this system, D1, D2, and D3 represent the distances between the carbonyl oxygen of ACh and the NH hydrogen of G121, G122, and A204, respectively. D4 and D5 respectively refer to the distances between the NH hydrogen of G121 and the oxygen atoms $O^{\varepsilon 1}$ and $O^{\varepsilon 2}$ of E202 side chain

are all reasonably close to the corresponding distances optimized at the HF/3-21G:Amber level, showing that the HF/3-21G level is adequate for the treatment of high-layer atoms in this study. This is consistent with the conclusion based on the earliest ab initio QM calculations [100] on the active site model. The earliest ab initio QM calculations [100] demonstrated that the HF/3-21G level is adequate for the geometry optimizations and that the energy barriers calculated at the B3LYP/6-31+G(d)//HF/3-21G level are all close to those calculated at the higher levels using the geometries optimized at the B3LYP/6-31G(d) level. Further, the QM/MM-optimized distances are also close to the corresponding distances in the MM-optimized structures, suggesting that it is reasonable using the classical force field for this kind of enzymatic reaction system.

It should be noted that the significance of the QM/MM calculations [115] described here is limited, because the geometries of the transition states were not fully optimized and, thus, the energy barriers cannot be evaluated explicitly based on these QM/MM calculations. More meaningful QM/MM reaction coordinate calculations [113] will be discussed later in this chapter.

The computational results summarized in Table 5 qualitatively confirm the existence of the oxyanion hole consisting of G116, G117, and A199 during BChE-catalyzed hydrolysis of cocaine, because G116, G117, and A199 all had hydrogen bonding or close interaction with O31 of cocaine in at least one transition state or intermediate. However, the N – H···O hydrogen bonds are mostly between cocaine O31 (i.e., the carbonyl oxygen at the benzoyl ester group) and the NH hydrogen atoms of G117 and A199. The NH hydrogen of G116 was not hydrogen-bonded to cocaine O31, except very briefly in INT2 and INT3. Only G117 had an N – H···O hydrogen bond with cocaine O31 in the MD-simulated prereactive BChE–cocaine complex ES. The simulated average H···O distance in this N – H···O hydrogen bond is 2.14 Å. After further energy minimization with Amber7 and the QM/MM geometry optimization, this H···O distance became 2.02 and 2.16 Å, respectively, as seen in Table 5. Changing from the prereactive complex (ES) to the transition states and intermediates, another N – H···O hydrogen bond formed between cocaine O31 and A199 while the N – H···O hydrogen bond with G117 was fully or partially maintained. For example, the N – H···O hydrogen bond between cocaine O31 and G117 existed partially in TS1 and fully in INT1. Thus, compared to ES, the transition states and intermediates were stabilized further by the hydrogen bonding of cocaine O31 with A199.

3.4.3 Hydrogen Bonding Energies

To better represent the overall strength of hydrogen bonding of cocaine O31 with the oxyanion hole in each MD-simulated structure, the total number of hydrogen bonds with cocaine O31 was estimated [115] by using a cut-

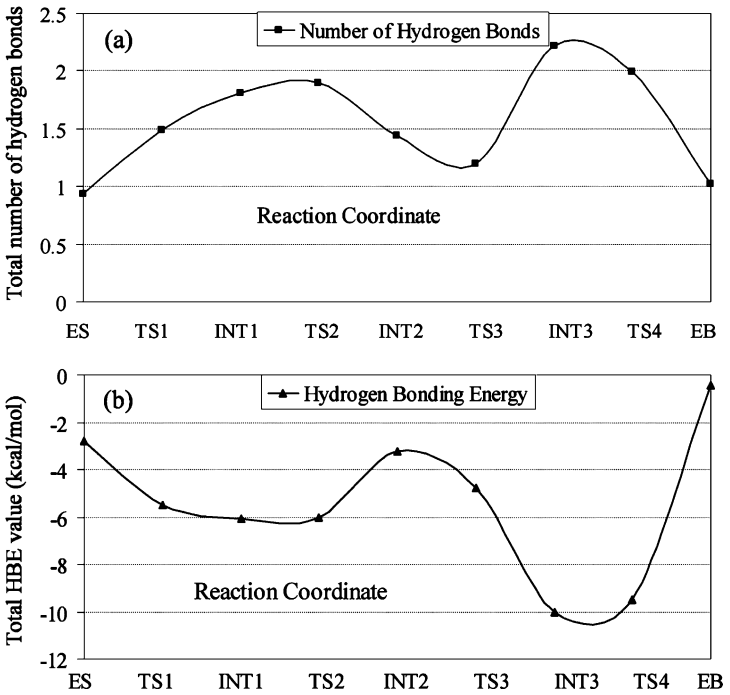

Fig. 8 Total average number of hydrogen bonds (**a**) and the corresponding total hydrogen bonding energy (**b**) between the carbonyl oxygen of cocaine benzoyl ester and the oxyanion hole in the simulated the prereactive BChE–cocaine complex (ES), transition states, intermediates, and product for BChE-catalyzed hydrolysis of (–)-cocaine [115]

off value of 2.5 Å for the H···O distances in order to roughly determine whether any hydrogen bond existed in any snapshot of MD simulation. Thus, the total number of hydrogen bonds with cocaine O31 can be obtained for each snapshot. The simulated total number of hydrogen bonds with cocaine O31 was estimated as the average over all of the snapshots taken in stable range of the MD trajectory. Figure 8a shows the simulated total numbers of hydrogen bonds estimated in this way for all of the structures involved in the reaction process: ES → TS1 → INT1 → TS2 → INT2 → TS3 → INT3 → TS4 → EB. Here, TS refer to the transition states, INT represent the intermediates, and EB refers to the BChE–benzoate acid complex. The results depicted in Fig. 8a clearly suggest that the total average number of hydrogen bonds between cocaine O31 and the oxyanion hole gradually increased from ES to TS1, INT1, and TS2, whereas the total average number of hydrogen bonds gradually decreased from TS2 to INT2 and TS3 before a remarkable increase from TS3 to INT3. In going from INT3 to TS4 and EB, the total average number of hydrogen bonds gradually decreased again.

As seen in Table 5, the H···O distances optimized at various levels of theory are consistent with the change of the simulated total average number of hydrogen bonds during the reaction process. For example, the optimized distances revealed only one N – H···O hydrogen bond with G117 in ES, a stronger N – H···O hydrogen bond with A199 and a weaker N – H···O hydrogen bond with G117 in TS1, and stronger N – H···O hydrogen bonds with both G117 and A199 in INT1. This supports the conclusion of the gradual increase of the hydrogen bonding for ES → TS1 → INT1.

With each of the simulated H···O distances, the hydrogen bonding energy (HBE) were also estimated by using the general HBE equation implemented in AutoDock 3.0 program suite [119]. Specifically, for each hydrogen bond with cocaine O31, a HBE value was evaluated with each snapshot of the MD-simulated structure. The final HBE of the MD-simulated hydrogen bond was considered to be the average HBE value of all snapshots taken from the stable MD trajectory. The total hydrogen bonding energy between cocaine O31 and the oxyanion hole in each MD-simulated state is depicted in Fig. 8b.

Comparing Fig. 8b with Fig. 8a, one can clearly see that the calculated total hydrogen bonding energy is mostly proportional to the simulated total number of hydrogen bonds, but the exception exists in some cases, particularly for the change from INT2 to TS3. The exception is due to the reason that different hydrogen bonds may have quite different average H···O distances and, therefore, have quite different hydrogen bonding energies. Thus, the total hydrogen bonding energy should be a better indicator of the overall hydrogen bonding between cocaine O31 and the oxyanion hole. In going from ES to TS1, the simulated total number of hydrogen bonds increases from 0.93 to 1.49 and, correspondingly, the calculated total HBE value changes from – 2.9 kcal/mol to – 5.5 kcal/mol, suggesting that the hydrogen bonding decreases the energy barrier for the first reaction step by ∼ 2.6 kcal/mol. In going from INT1 to TS2, the simulated total number of hydrogen bonds changes from 1.81 to 1.90 and the calculated total HBE value changes from – 6.1 kcal/mol to – 6.0 kcal/mol, indicating that the hydrogen bonding effects on the energy barrier for the second reaction step are negligible. In going from INT2 to TS3, the simulated total number of hydrogen bonds decreases from 1.44 to 1.20, whereas the calculated total HBE value changes from – 3.2 kcal/mol to – 4.8 kcal/mol, showing that the average hydrogen bonding strength per bond in TS3 is stronger than that in INT2. These energetic data suggest that the hydrogen bonding effects might decrease the energy barrier for the third reaction step by ∼ 1.6 kcal/mol. In going from INT3 to TS4, the simulated total number of hydrogen bonds decreases from 2.22 to 1.99 and the calculated total HBE value changes from – 10.1 kcal/mol to – 9.5 kcal/mol, suggesting that the hydrogen bonding may slightly increase the energy barrier for the fourth reaction step by ∼ 0.6 kcal/mol.

3.4.4
Comparison with AChE-Catalyzed Hydrolysis of Acetylcholine

It is interesting to compare the mechanism of BChE-catalyzed hydrolysis of cocaine with that of AChE-catalyzed hydrolysis of neurotransmitter acetylcholine (ACh), because AChE and BChE have very similar active sites including the same type of catalytic triad and the same type of oxyanion hole. In terms of mouse AChE, the catalytic triad consists of S203, H447, and E334 and the oxyanion hole consists of G121, G122, and A204. The only significant difference is that the cavity of BChE active site is larger so that it can accommodate a larger substrate like cocaine. McCammon et al. [120–122] reported MD simulations and QM/MM calculations on the mouse AChE–ACh system. Their MD simulations [121, 122] were performed on the prereactive AChE–ACh complex, whereas their QM/MM calculations [120] were carried out on the initial step of the acylation stage of the AChE-catalyzed ACh hydrolysis. Their QM/MM results [120] indicate that in the AChE–ACh Michaelis complex, two hydrogen bonds exist between the carbonyl oxygen of ACh and the peptidic NH groups of G121 and G122. In going from the AChE–ACh Michaelis–Menten complex to the (first) transition state and (first) intermediate, the distance between the carbonyl oxygen of ACh and NH group of A204 becomes shorter, and the third hydrogen bond is formed both in the transition state and in the tetrahedral intermediate [120]. Based on the structural similarity of these two closely related cholinesterases, one might easily assume that the N – H···O hydrogen bonding between the carbonyl oxygen of the substrate and the three residues of oxyanion hole in the BChE–cocaine and AChE–ACh systems should be very close to each other during the catalytic hydrolysis processes. However, a remarkable difference exists on the role of the first residue, i.e., G121 in AChE or G116 in BChE, of the oxyanion hole. The MD simulations and QM/MM calculations [115] on BChE-catalyzed cocaine hydrolysis revealed that G116 never hydrogen-bonded to O31 of cocaine during the acylation stage and was rarely involved in hydrogen bonding with O31 of cocaine during the deacylation stage. The simulated structures ES, TS1, INT1, and TS2 [115] are associated with the acylation stage, in which all of the cocaine atoms were included in the simulations and calculations. The simulated structures INT2, TS3, INT3, and TS4 are all associated with the deacylation stage, in which the free product ecgonine methyl ester had left the active site and cocaine only had benzoate atoms included in the simulations and calculations.

To make sure that this remarkable difference between the structures simulated for these two hydrolysis processes was not an artifact of the possibly different computational strategies used for the two different reaction processes, the prereactive complex between ACh and mouse AChE (using X-ray crystal structure 1MAH in the Protein Data Bank [123]) was also simulated by using the same MD approach as used for the BChE–cocaine system. As

seen in Table 5, the MD simulation of the prereactive AChE–ACh complex also revealed an N – H···O hydrogen bond between the carbonyl oxygen of ACh and the NH hydrogen of G121, which is qualitatively consistent with the computational results reported by McCammon et al. [120–122]. This consistency supports the remarkable difference between the two catalytic hydrolysis processes.

To further examine the possible effect of the bulky ligand (cocaine) on the hydrogen bond between G116 and E197, an additional MD simulation [115] on BChE was carried out in a water bath without cocaine or any other ligand. As seen in Table 5, the simulated BChE structure did not show a hydrogen bond between G116 and E197, showing that the ligand has a role in the hydrogen bonding between the NH hydrogen of G116 and the carboxyl group of E197 side chain.

3.5
Effects of Protein Environment on the Energy Barriers

The key to the rational design of high-activity mutants of BChE against (–)-cocaine is to further understand the protein environmental effects on the reaction pathway, particularly the transition states involved and the corresponding energy barriers. This is because, to increase the catalytic activity of BChE for (–)-cocaine, one needs to design necessary mutation(s) to modify the protein environment such that the modified protein environment can more favorably stabilize the transition states and, therefore, lower the energy barriers, particularly for the rate-determining step(s). Understanding the protein environmental effects on the reaction pathway and energy barriers should help to rationally design BChE mutants with a lower energy barrier and, therefore, a higher catalytic activity for (–)-cocaine. However, ab initio reaction coordinate calculations [100] with an active site model can only account for breaking and formation of covalent bonds during the catalytic reaction process; the more complex protein environmental effects on the reaction pathway and energy barriers cannot be accounted for very well. Recently, extensive hybrid quantum mechanical/molecular mechanical (QM/MM) calculations [113] were performed on the entire BChE-(–)-cocaine and BChE-(+)-cocaine systems to optimize the geometries of the transition states and the corresponding prereactive enzyme–substrate complexes and of intermediates involved in the BChE-catalyzed hydrolysis of (–)- and (+)-cocaine, and to predict the corresponding energy barriers. The calculated results reveal remarkable effects of the protein environment on the energy barriers and provide useful insights into rational design of BChE mutants with lower energy barriers for the catalytic hydrolysis of (–)-cocaine.

3.5.1 QM/MM-Optimized Geometries of Transition States

The geometry optimizations using the QM/MM method have led to the converged geometries of the transition states (TS1, TS2, TS3, and TS4) and the corresponding prereactive BChE–cocaine complex (ES) and intermediates (INT1, INT2, and INT3) for the hydrolyses of (–)- and (+)-cocaine catalyzed by human BChE (see Scheme 1 for the atoms treated quantum mechanically in the QM/MM calculations) [113]. The QM/MM-optimized geometries [113] of the transition states, intermediates, and prereactive BChE–cocaine complex and their connections on the potential energy surface are consistent with the assumed enzymatic reaction pathway involving four reaction steps depicted in Scheme 1. For example, in the first step associated with TS1, the hydroxyl oxygen of S198 gradually attacks the carbonyl carbon of cocaine benzoyl ester, while the proton of the hydroxyl group gradually transfers to a nitrogen atom of H438 side chain, and the H438 side chain gradually transfers another proton to an oxygen atom of E325 side chain. This reaction step and the third reaction step (associated with TS3) both belong to the standard general base-catalysis mechanism, whereas both the second and fourth steps (associated with TS2 and TS4) follow the standard specific acid-catalysis mechanism. The results obtained from the QM/MM calculations qualitatively confirm the fundamental reaction pathway proposed for BChE-catalyzed hydrolysis of cocaine based on the earliest reaction coordinate calculations with a simplified active site model [100]. It follows that the protein environment neglected in the earliest reaction coordinate calculations do not change the fundamental reaction pathway for this enzymatic reaction, as far as the breaking and formation of covalent bonds are concerned.

However, the protein environment significantly affects the hydrogen bonding between the carbonyl oxygen of cocaine and the oxyanion hole (G116, G117, and A199) during the enzymatic reaction process [113]. Such type of hydrogen bonding with the oxyanion hole is crucial for the transition state stabilization, particularly for the first and third reaction steps, because the carbonyl oxygen atom in TS1 and TS3 possesses more negative charge than that in ES and INT2. The key internuclear distances concerning the hydrogen bonding in the QM/MM-optimized geometries of the transition states are all qualitatively consistent with those summarized in Table 5.

3.5.2 Energy Barriers

Table 6 summarizes the energy barriers predicted for BChE-catalyzed hydrolysis of (–)- and (+)-cocaine by performing the QM/MM calculations at the MP2/6-31+G(d):Amber level for all of the reaction steps, along with the corresponding energy barriers calculated for the (–)-cocaine hydrolysis with

Table 6 Energy barriers (ΔE_a, in kcal/mol) calculated for BChE-catalyzed hydrolysis of (–)- and (+)-cocaine [113]

Method and substrate		ΔE_a Step 1	Step 2	Step 3	Step 4
Neglecting protein environment[a]	(–)-Cocaine	4.0	3.1	16.6 (17.0)	6.5
Including protein environment[b]	(–)-Cocaine	13.0	0.1	14.2	7.2
	(+)-Cocaine	12.1	0.4	14.2	7.2

[a] Calculated for a simplified model system [100] at the MP2/6-31+G(d)//HF/3-21G level. The value in parenthesis was calculated at the MP2/6-31+G(d)//B3LYP/6-31G(d) level

[b] Calculated for the real enzymatic reaction system by using the QM/MM method at the MP2/6-31+G(d):Amber level with the geometries optimized at the HF/3-21G:Amber level

a simplified active site model of BChE (neglecting the protein environment) for comparison. A comparison between the two sets of energy barriers listed in Table 6 reveals that the protein environmental effects dramatically change the energy barrier calculated for the first reaction step of the (–)-cocaine hydrolysis. The energy barriers calculated for the other steps are relatively less sensitive to the inclusion of the protein environment. The protein environmental effects increase the energy barrier for the first step of the (–)-cocaine hydrolysis by ~ 9 kcal/mol, decrease the energy barriers for the second and third steps by ~ 2–3 kcal/mol, and slightly increase the energy barrier for the fourth step. As a result, the second reaction step becomes almost barrierless and the energy barrier calculated for the fourth step is still much lower than that calculated for the third step. Based on the QM/MM results listed in Table 6, the third reaction step has the highest energy barrier, 14.2 kcal/mol; the energy barrier of 13.0 kcal/mol calculated for the first step of the (–)-cocaine hydrolysis is close to the barrier calculated for the third step. The energy barrier of 12.1 kcal/mol calculated for the first step of the (+)-cocaine hydrolysis is slightly lower than that the first step of the (–)-cocaine hydrolysis.

Note that the third and fourth reaction steps of BChE-catalyzed hydrolysis of (+)-cocaine are the same as the corresponding third and fourth reaction steps of BChE-catalyzed hydrolysis of (–)-cocaine. The highest energy barrier being associated with the third step means that (–)- and (+)-cocaine should be hydrolyzed by BChE at the same rate if the chemical reaction process is the rate-determining stage for both (–)- and (+)-cocaine. Further, if the chemical reaction process is the rate-determining stage, the catalytic rate constant k_{cat} should be dependent on the pH of the reaction solution, because H438 in the catalytic triad can be protonated and lose its catalytic role at low pH. However, BChE-catalyzed hydrolysis of (+)-cocaine ($k_{cat} = 1.07 \times 10^2\ s^{-1}$ and $K_M = 8.5\ \mu M$) was observed to be three

orders-of-magnitude faster than BChE-catalyzed hydrolysis of (–)-cocaine ($k_{cat} = 6.5 \times 10^{-2}$ s^{-1} and $K_M = 9.0$ μM) [97] and only the k_{cat} value for (+)-cocaine was pH-dependent. So, the experimental data [97] clearly indicate that the rate-determining stage should be the chemical reaction process for (+)-cocaine, whereas the formation of the prereactive BChE-substrate binding complex (ES) should be the rate determining stage for (–)-cocaine. The calculated energy barriers further demonstrate that the third reaction step is the rate-determining step for (+)-cocaine.

The highest energy barrier calculated for BChE-catalyzed cocaine hydrolysis is ~ 3.7 kcal/mol higher than that (10.5 kcal/mol) calculated at the similar level, i.e., MP2/6-31+G(d) QM/MM, by McCammon et al. [120] for the first step of the AChE-catalyzed hydrolysis of ACh (the first step was recognized as the rate-determining step for the enzymatic reaction). The difference in the energy barrier between the two enzymatic reactions can be attributed to the aforementioned difference in the number of N – H···O hydrogen bonds of the substrate with the oxyanion hole of the enzyme during the reaction processes.

The difference between the QM/MM-calculated energy barriers for the rate-determining steps of the two enzymatic reaction systems is consistent with the experimental observation that the k_{cat} value (1.6×10^4 s^{-1}) [124] for AChE-catalyzed hydrolysis of ACh was about 150-fold larger than that ($k_{cat} = 1.07 \times 10^2$ s^{-1}) [97] for BChE-catalyzed hydrolysis of (+)-cocaine. Based on the widely used classical transition-state theory (CTST) [125], the experimental k_{cat} difference of ~ 150-fold suggests an energy barrier difference of ~ 3.0 kcal/mol when $T = 298.15$ K, which is in good agreement with the calculated barrier difference of ~ 3.7 kcal/mol [113].

3.5.3 Insights into Rational Design of BChE Mutants

It has been known that the formation of the prereactive BChE-(–)-cocaine complex (ES) is the rate-determining step of BChE-catalyzed hydrolysis of (–)-cocaine. Hence, the earliest rational design of BChE mutants has been focused on how to accelerate the ES formation process; for example, A328W/Y332A mutant of BChE was found to have a ~ 9.4-fold improved catalytic efficiency (k_{cat}/K_M) against (–)-cocaine [98, 99]. However, it was not clear whether the energy barrier for the first step of BChE-catalyzed hydrolysis of (–)-cocaine is higher than that for the third step or not. If the energy barrier for the first step were significantly higher than that for the third step, it would mean that the catalytic efficiency of BChE against (–)-cocaine should still be significantly lower than that against (+)-cocaine, even if the chemical reaction process became rate determining. In that case, the site-directed mutagenesis designed to only speedup the ES formation process can be expected to make a limited improvement of the catalytic efficiency against (–)-cocaine. If the energy barrier for the third reaction step were

the highest within the chemical reaction process, the catalytic efficiency of BChE against (–)-cocaine would be the same as that against (+)-cocaine when the chemical reaction process became rate determining. The energy barriers determined by the QM/MM calculations on BChE-catalyzed hydrolyses of (–)- and (+)-cocaine further demonstrate that the third reaction step indeed has the highest energy barrier (14.2 kcal/mol) within the chemical reaction processes, but the energy barrier of 13.0 kcal/mol calculated for the first step of (–)-cocaine hydrolysis is close to that for the third step. Further, the energy barrier for the first step is rather sensitive to the change of the protein environment because the protein environmental effects dramatically increase the energy barrier calculated for the first step, although the energy barriers for the subsequent steps look less sensitive to the change of the protein environment. These computational results suggest that it would be possible to design a BChE mutant that has a catalytic efficiency against (–)-cocaine comparable to wild-type BChE against (+)-cocaine, if the designed mutation could considerably speedup the ES formation process without significantly changing the energy barrier for any step of the chemical reaction process. However, a mutation designed to speedup the ES formation process could also change the energy barriers for the chemical reaction steps, especially for the first reaction step because the energy barrier calculated for this step is so sensitive to the protein environmental effects. So, future rational design of the high activity mutants of BChE against (–)-cocaine should pay attention to whether the mutation could also increase or decrease the energy barrier(s) for the first and/or third step of the chemical reaction process.

These computational insights help to understand available experimental data better. It has been found that the catalytic rate constant k_{cat} of A328W/Y332A BChE is pH-dependent for both (–)- and (+)-cocaine hydrolyses and that the A328W/Y332A mutation does not change the catalytic efficiency against (+)-cocaine [99]. The experimental kinetic data show that the chemical reaction process becomes the rate-determining for both (–)- and (+)-cocaine hydrolyses catalyzed by A328W/Y332A mutant of BChE, but the energy barriers for the rate-determining step of the two reactions must be different. Taking these experimental data and QM/MM results into account together, it is very likely that the rate-determining step of (+)-cocaine hydrolysis catalyzed by A328W/Y332A mutant of BChE is still the third reaction step. However, the rate-determining step of (–)-cocaine hydrolysis catalyzed by A328W/Y332A mutant of BChE becomes the first reaction step and has a significantly higher energy barrier than the third step. A closer look [113] at the detailed TS1 structure optimized for hydrolysis of (–)-cocaine catalyzed by wild-type BChE reveals that the TS1 structure is likely stabilized by a cation-π interaction between the protonated tropane nitrogen of (–)-cocaine and the benzene ring of Y332 side chain. The QM/MM-optimized distance between the protonated tropane nitrogen of (–)-cocaine and the center of the benzene ring of Y332 side chain was $\sim$ 4.9 Å. Such a cation-π interaction will disap-

pear when Y332 changes to Ala. Hence, while the Y332A mutation can help to remove the hindrance for the ES formation, the Y332A mutation may also destabilize the TS1 structure for (–)-cocaine hydrolysis. The Y332A mutation having no significant effect on the third reaction step may be explained by the fact that the tropane group of (–)-cocaine has left the active site after the second reaction step. Thus, there is no cation-π interaction in the TS3 structure whether Y332 changes to Ala or not. This mechanistic understanding suggests that starting from A328W/Y332A mutant of BChE, the rational design of further mutation(s) to improve the catalytic activity against (–)-cocaine should primarily aim to decrease the energy barrier for the first reaction step without significantly affecting the ES formation and other chemical reaction steps.

3.6 Computational Design of BChE Mutants Based on Transition State Simulations

Generally speaking, for rational design of a mutant enzyme with a higher catalytic activity for a given substrate, one needs to design a mutation that can accelerate the rate-determining step of the entire catalytic reaction process while the other steps are not slowed down by the mutation. As discussed above, extensive computational modeling and experimental data indicate that the formation of the prereactive BChE-(–)-cocaine complex (ES) is the rate-determining step of (–)-cocaine hydrolysis catalyzed by wild-type BChE [97–101], whereas the rate-determining step of the corresponding (+)-cocaine hydrolysis is the chemical reaction process consisting of the acylation and deacylation stages, or four individual reaction steps [113]. This mechanistic understanding is consistent with the experimental observation [99] that the catalytic rate constant of wild-type BChE against (+)-cocaine is pH-dependent, whereas that of the same enzyme against (–)-cocaine is independent of the pH. The pH-dependence of the rate constant for (+)-cocaine hydrolysis is clearly associated with the protonation of H438 residue in the catalytic triad (S198, H438, and E325). For the first and third steps of the reaction process, when H438 is protonated, the catalytic triad cannot function and, therefore, the enzyme becomes inactive. The lower the pH of the reaction solution, the higher the concentration of the protonated H438, and the lower the concentration of the active enzyme. Hence, the rate constant was found to decrease with decreasing the pH of the reaction solution for the enzymatic hydrolysis of (+)-cocaine [99].

Based on the above mechanistic understanding, the earlier efforts for rational design of the BChE mutants were focused on how to improve the ES formation process. Several BChE mutants [97–99, 101, 114], including A328W, A328W/Y332A, A328W/Y332G, and F227A/S287G/A328W/Y332M, have been found to have a significantly higher catalytic efficiency (k_{cat}/K_M) against (–)-cocaine; these mutants of BChE have a $\sim$ nine- to 34-fold improved catalytic

efficiency against (–)-cocaine. The aforementioned analysis of experimental and computational data clearly shows that the rate-determining step of (–)-cocaine hydrolysis catalyzed by the A328W/Y332A mutant should be the first step of the chemical reaction process. Further, recently reported computational modeling [97–101] also suggests that the formation of the prereactive BChE-(–)-cocaine complex (ES) is hindered mainly by the bulky side chain of Y332 residue in wild-type BChE, but the hindering can be removed by the Y332A or Y332G mutation [101, 117]. Therefore, starting from the A328W/Y332A or A328W/Y332G mutant, the rational design of further mutation(s) to improve the catalytic efficiency of BChE against (–)-cocaine can aim to decrease the energy barrier for the first reaction step without significantly affecting the ES formation and other chemical reaction steps [117].

For rational design of high-activity mutants of BChE, a unique computational strategy [117] has been developed to virtually screen various possible BChE mutants based on MD simulations of the rate-determining transition state (i.e., TS1).

In the design of a high-activity mutant of BChE against (–)-cocaine, one would like to predict some possible mutations that can lower the energy of the transition state for the first chemical reaction step (TS1) and, therefore, lower the energy barrier for this critical reaction step. Apparently, a mutant associated with the stronger hydrogen bonding between the carbonyl oxygen of (–)-cocaine benzoyl ester and the oxyanion hole of the BChE mutant in the TS1 structure may potentially have a more stable TS1 structure and, therefore, a higher catalytic efficiency for (–)-cocaine hydrolysis. Hence, the hydrogen bonding with the oxyanion hole in the TS1 structure is a crucial factor affecting the transition state stabilization and the catalytic activity. The possible effects of some mutations on the hydrogen bonding were examined by performing MD simulations on the TS1 structures for (–)-cocaine hydrolysis catalyzed by wild-type BChE and its various mutants [117]. The MD simulation in water was performed for 1 ns or longer to make sure a stable MD trajectory was obtained for each simulated TS1 structure with wild-type or mutant BChE. Figure 9 depicts plots of four important H···O distances in the MD-simulated TS1 structure versus the simulation time for (–)-cocaine hydrolysis catalyzed by A199S/S287G/A328W/Y332G BChE, along with the root-mean-square deviation (RMSD) of the simulated positions of backbone atoms from those in the corresponding initial structure. The H···O distances in the simulated TS1 structures for wild-type BChE and its three mutants are summarized in Table 7. The H···O distances between the carbonyl oxygen of (–)-cocaine and the peptidic NH hydrogen atoms of G116, G117, and A199 (or S199) of BChE are denoted by D1, D2, and D3, respectively, in Table 7 and Fig. 9. D4 in Table 7 and Fig. 9 refers to the H···O distance between the carbonyl oxygen of (–)-cocaine and the hydroxyl hydrogen of S199 side chain in the simulated TS1 structure corresponding to the A199S/S287G/A328W/Y332G mutant.

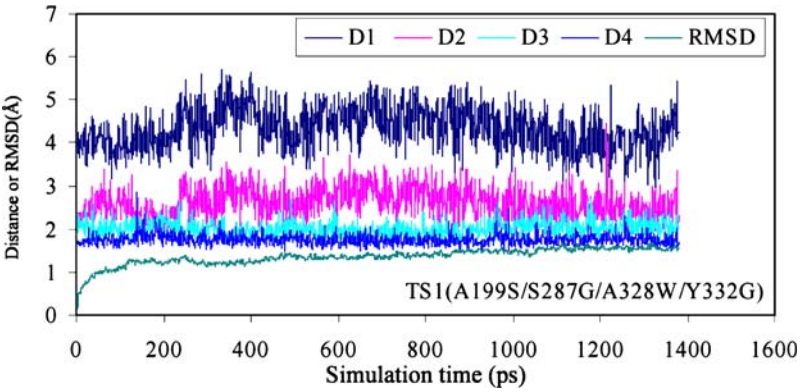

Fig. 9 Plots of the key internuclear distances (in Å) versus the time in the simulated TS1 structure for (–)-cocaine hydrolysis catalyzed by A199S/S287G/A328W/Y332G BChE [117]. Traces *D*1, *D*2, and *D*3 refer to the distances between the carbonyl oxygen of (–)-cocaine and the NH hydrogen of G116, G117, and S199, respectively. Trace *D*4 is the internuclear distance between the carbonyl oxygen of (–)-cocaine and the hydroxyl hydrogen of the S199 side chain in A199S/S287G/A328W/Y332G BChE. RMSD represents the root-mean-square deviation (in Å) of the simulated positions of the protein backbone atoms from those in the initial structure

As seen in Table 7, the simulated H···O distance D1 is always too long for the peptidic NH of G116 to form a N – H···O hydrogen bond with the carbonyl oxygen of (–)-cocaine in all of the simulated TS1 structures. In the simulated TS1 structure for wild-type BChE, the carbonyl oxygen of (–)-cocaine formed a firm N – H···O hydrogen bond with the peptidic NH hydrogen atom of A199 residue; the simulated H···O distance (D3) was 1.61 to 2.35 Å, with an average D3 value of 1.92 Å. Meanwhile, the carbonyl oxygen of (–)-cocaine also had a partial N – H···O hydrogen bond with the peptidic NH hydrogen atom of G117 residue; the simulated H···O distance (D2) was 1.97 to 4.14 Å (the average D2 value was 2.91 Å). The average D2 and D3 values became 2.35 and 1.95 Å, respectively, in the simulated TS1 structure for the A328W/Y332A mutant. These distances suggest a slightly weaker N – H···O hydrogen bond with A199, but a stronger N – H···O hydrogen bond with G117, in the simulated TS1 structure for the A328W/Y332A mutant that the corresponding N – H···O hydrogen bonds for the wild-type. The average D2 and D3 values (2.25 and 1.97 Å, respectively) in the simulated TS1 structure for the A328W/Y332G mutant are close to the corresponding distances for the A328W/Y332A mutant. The overall strength of the hydrogen bonding between the carbonyl oxygen of (–)-cocaine and the oxyanion hole of the enzyme is not expected to change considerably when wild-type BChE is replaced by the A328W/Y332A or A328W/Y332G mutant.

However, the story for the simulated TS1 structure for (–)-cocaine catalyzed by the A199S/S287G/A328W/Y332G mutant was remarkably different.

Table 7 Summary of the MD-simulated key distances (in Å) and the calculated total hydrogen-bonding energies (HBE, in kcal/mol) between the oxyanion hole and the carbonyl oxygen of (–)-cocaine benzoyl ester in the first transition state (TS1) [117]

Transition state	Distance[a]	D1	D2	D3	D4	Total HBE[b]
TS1 structure for (–)-cocaine hydrolysis catalyzed by wild-type BChE	Average	4.59	2.91	1.92		– 5.5 (– 4.6)
	Maximum	5.73	4.14	2.35		
	Minimum	3.35	1.97	1.61		
	Fluctuation	0.35	0.35	0.12		
TS1 structure for (–)-cocaine hydrolysis catalyzed by A328W/Y332A mutant of BChE	Average	3.62	2.35	1.95		– 6.2 (– 4.9)
	Maximum	4.35	3.37	3.02		
	Minimum	2.92	1.78	1.61		
	Fluctuation	0.23	0.27	0.17		
TS1 structure for (–)-cocaine hydrolysis catalyzed by A328W/Y332G mutant of BChE	Average	3.60	2.25	1.97		– 6.4 (– 5.0)
	Maximum	4.24	3.17	2.76		
	Minimum	2.89	1.77	1.62		
	Fluctuation	0.23	0.24	0.17		
TS1 structure for (–)-cocaine hydrolysis catalyzed by A199S/S287G/A328W/Y332G mutant of BChE	Average	4.39	2.60	2.01	1.76	– 14.0 (– 12.0)
	Maximum	5.72	4.42	2.68	2.50	
	Minimum	2.87	1.76	1.62	1.48	
	Fluctuation	0.48	0.36	0.17	0.12	

[a] D1, D2, and D3 represent the internuclear distances between the carbonyl oxygen of cocaine benzoyl ester and the NH hydrogen of residues #116 (i.e. G116), #117 (i.e. G117), and #199 (i.e. A199 or S199) of BChE, respectively. D4 is the internuclear distance between the carbonyl oxygen of cocaine benzoyl ester and the hydroxyl hydrogen of S199 side chain in the A199S/S287G/A328W/Y332G mutant

[b] Total HBE value is the average of the HBE values calculated by using the instantaneous distances in all of the snapshots. The value in parenthesis is the total HBE value calculated by using the MD-simulated average distances

As one can see from Table 7 and Fig. 9, when residue #199 becomes a serine (i.e., S199), the hydroxyl group on the side chain of S199 can also hydrogen-bond to the carbonyl oxygen of (–)-cocaine to form an O – H···O hydrogen bond, in addition to the two N – H···O hydrogen bonds with the peptidic NH of G117 and S199. The simulated average H···O distances with the peptidic NH hydrogen of G117, peptidic NH hydrogen of S199, and hydroxyl hydrogen of S199 are 2.60, 2.01, and 1.76 Å, respectively. Due to the additional O – H···O hydrogen bond, the overall strength of the hydrogen bonding with the modified oxyanion hole of A199S/S287G/A328W/Y332G BChE should be significantly stronger than that of wild-type, A328W/Y332A, and A328W/Y332G BChEs.

To better represent the overall strength of hydrogen bonding between the carbonyl oxygen of (–)-cocaine and the oxyanion hole in a MD-simulated TS1

structure, the hydrogen bonding energy (HBE) associated with each simulated H···O distance was estimated [117]. For each hydrogen bond with the carbonyl oxygen of (–)-cocaine, a HBE value can be evaluated with each snapshot of the MD-simulated structure. The final HBE of the MD-simulated hydrogen bond is considered to be the average HBE value of all snapshots taken from the stable MD trajectory. The estimated total HBE value for the hydrogen bonds between the carbonyl oxygen of (–)-cocaine and the oxyanion hole in each simulated TS1 structure is also shown in Table 7.

The HBE for each hydrogen bond was also estimated by using the MD-simulated average H···O distance. As seen in Table 7, the total hydrogen-bonding energies (i.e., – 4.6, – 4.9, – 5.0, and – 12.0 kcal/mol for the wild-type, A328W/Y332A, A328W/Y332G, and A199S/S287G/A328W/Y332G BChEs, respectively) estimated in this way are systematically higher (i.e., less negative) than the corresponding total hydrogen-bonding energies (i.e., – 5.5, – 6.2, – 6.4, and – 14.0 kcal/mol) estimated in the aforementioned way. However, the two sets of total HBE values are qualitatively consistent with each other in terms of the relative hydrogen-bonding strengths in the four simulated TS1 structures. In particular, the two sets of total HBE values consistently reveal that the overall strength of the hydrogen bonding between the carbonyl oxygen of (–)-cocaine and the oxyanion hole in the simulated TS1 structure for A199S/S287G/A328W/Y332G BChE is significantly stronger than that for wild-type, A328W/Y332A, and A328W/Y332G BChEs.

The computational results discussed above suggest that the transition state for the first chemical reaction step (TS1) of (–)-cocaine hydrolysis catalyzed by the A199S/S287G/A328W/Y332G mutant should be significantly more stable than that by the A328W/Y332A or A328W/Y332G mutant, due to the significant increase of the overall hydrogen bonding between the carbonyl oxygen of (–)-cocaine and the oxyanion hole of the enzyme in the TS1 structure. The aforementioned analysis of the literature also indicates that the first chemical reaction step associated with TS1 should be the rate-determining step of (–)-cocaine hydrolysis catalyzed by a BChE mutant including Y332A or Y332G mutation, although the formation of the prereactive enzyme–substrate complex (ES) is the rate-determining step for (–)-cocaine hydrolysis catalyzed by wild-type BChE. This suggests a clear correlation between the TS1 stabilization and the catalytic efficiency of A328W/Y332A, A328W/Y332G, and A199S/S287G/A328W/Y332G BChEs for (–)-cocaine hydrolysis: the more stable the TS1 structure, the lower the energy barrier, and the higher the catalytic efficiency. Thus, the MD simulations predict that A199S/S287G/A328W/Y332G BChE should have a higher catalytic efficiency than A328W/Y332A or A328W/Y332G BChE for (–)-cocaine hydrolysis.

The computational predictions based on the transition state simulations were followed by wet experiments [117]. The wet experiments have revealed that A199S/S287G/A328W/Y332G BChE has a ∼ 456-fold im-

proved catalytic efficiency against (–)-cocaine compared to the wild-type, or A199S/S287G/A328W/Y332G BChE has a k_{cat}/K_M value of $\sim (4.15 \pm 0.37) \times 10^8\ M\ min^{-1}$ for (–)-cocaine hydrolysis [117]. The catalytic efficiency of A199S/S287G/A328W/Y332G BChE against (–)-cocaine is significantly higher than that of AME-359 (i.e., F227A/S287G/A328W/Y332M BChE, $k_{cat}/K_M = 3.1 \times 10^7\ M\ min^{-1}$), whose catalytic efficiency against (–)-cocaine is the highest within all of the previously reported BChE mutants) [114]. AME-359 has a $\sim$ 34-fold improved catalytic efficiency against (–)-cocaine compared to wild-type BChE. By using the designed A199S/S287G/A328W/Y332G BChE as an exogenous enzyme in humans, when the concentration of this mutant is kept the same as that of the wild-type BChE in plasma, the halflife of (–)-cocaine in plasma should be reduced from $\sim$ 45–90 min to only $\sim$ 6–12 s, considerably shorter than the time required for cocaine to cross the blood–brain barrier to reach the CNS. Hence, the outcome of the rational design and discovery study could eventually result in a valuable, efficient anti-cocaine medication.

4 Concluding Remarks

Reaction mechanisms of cocaine hydrolysis have been studied extensively through the combined use of a variety of state-of-the-art techniques of molecular modeling. The computational techniques used include homology modeling, molecular docking, molecular dynamics simulations, first-principles electronic structure calculations, and hybrid quantum mechanical/molecular mechanical calculations. These state-of-the-art computational studies have led to detailed mechanistic insights into the reaction pathways and energy profiles for non-enzymatic hydrolysis of cocaine in water and for cocaine hydrolysis catalyzed by human butyrylcholinesterase (BChE). These detailed mechanistic insights provide a solid basis for rational design of possible anti-cocaine medication. In particular, the information about the transition states and their stabilization for non-enzymatic hydrolysis of cocaine in water has been very useful in rational design of stable analogs of the transition states for cocaine hydrolysis to elicit new anti-cocaine catalytic antibodies. By using the computational insights into the catalytic mechanisms for BChE-catalyzed hydrolysis of (–)- and (+)-cocaine, a novel computational design strategy based on the simulation of the rate-determining transition state has been developed to design high-activity mutants of BChE for hydrolysis of (–)-cocaine. This has led to the exciting discovery of BChE mutants with considerably improved catalytic efficiency against (–)-cocaine. One of the discovered new BChE mutants (i.e., A199S/S287G/A328W/Y332G) has a $\sim$ 456-fold improved catalytic efficiency against (–)-cocaine. The encouraging outcome of the computational design

and discovery effort demonstrates that the unique computational design approach based on transition-state simulation holds promise for rational enzyme redesign and drug discovery.

Concerning future directions of the mechanism-based design of anti-cocaine therapeutic, the catalytic efficiency of BChE could be improved further by continuing use of the novel computational design strategy followed by wet experimental tests. The catalytic efficiency of the discovered anti-cocaine catalytic antibodies could also be improved through computational design of possible mutants of the catalytic antibodies. For this purpose, one first needs to understand the detailed catalytic mechanisms for (–)-cocaine hydrolysis catalyzed by the catalytic antibodies and then see how to stabilize the rate-determining transition state for the hydrolysis process. The similar computational protocols that have been used for BChE and its mutants can be employed to study the catalytic mechanism of cocaine hydrolysis catalyzed by the catalytic antibodies and to design their possible high-activity mutants. In addition to high-activity mutants of BChE and catalytic antibodies, one may also consider the alternative options of developing high-activity mutants of other enzymes for accelerating (–)-cocaine metabolism. The similar computational protocols used for BChE and its mutants can also be employed to study the catalytic mechanisms of cocaine hydrolysis catalyzed by other enzymes and to design their possible high-activity mutants.

Finally, the similar computational strategy discussed in this chapter in combination with appropriate wet experiments may also be useful in rational redesign of many other metabolic enzymes for the therapeutic treatments of metabolic diseases.

Acknowledgements The financial support from the National Institute on Drug Abuse (NIDA) of the National Institutes of Health (NIH) (grant R01 DA013930) is gratefully acknowledged.

References

1. Gawin FH, Ellinwood EHN Jr (1988) Eng J Med 318:1173
2. Landry DW (1997) Sci Am 276:28
3. Singh S (2000) Chem Rev 100:925
4. Sparenborg S, Vocci F, Zukin S (1997) Drug Alcohol Depend 48:149
5. Gorelick DA (1997) Drug Alcohol Depend 48:159
6. Gorelick DA, Gardner EL, Xi ZX (2004) Drugs 64:1547
7. Baird TJ, Deng SX, Landry DW, Winger G, Woods JH (2000) J Pharmacol Exp Ther 295:1127
8. Carrera MRA, Ashley JA, Wirsching P, Koob GF, Janda KD (2001) Proc Natl Acad Sci USA 98:1988
9. Deng SX, de Prada P, Landry DW (2002) J Immunol Methods 269:299
10. Kantak KM (2003) Expert Opin Pharmacother 4:213

11. Carrera MRA, Kaufmann GF, Mee JM, Meijler MM, Koob GF, Janda KD (2004) Proc Natl Acad Sci USA 101:10416
12. Dickerson TJ, Kaufmann GF, Janda KD (2005) Expert Opin Biol Ther 5:773
13. Meijler MM, Kaufmann GF, Qi LW, Mee JM, Coyle AR, Moss JA, Wirsching P, Matsushita M, Janda KD (2005) J Am Chem Soc 127:2477
14. Rogers CJ, Mee JM, Kaufmann GF, Dickerson TJ, Janda KD (2005) J Am Chem Soc 127:10016
15. Carrera MRA, Ashley JA, Parsons LH, Wirsching P, Koob GF, Janda KD (1995) Nature 378:727
16. Fox BS (1997) Drug Alcohol Depend 100:153
17. Carrera MRA, Ashley JA, Zhou B, Wirsching P, Koob GF, Janda KD (2000) Proc Natl Acad Sci USA 97:6202
18. Carrera MRA, Ashley JA, Wirsching P, Koob GF, Janda KD (2001) Proc Natl Acad Sci USA 98:1988
19. Carrera MRA, Trigo JM, Roberts AJ, Janda KD (2005) Pharmacol Biochem Behav 81:709
20. Fox BS, Kantak KM, Edwards MA, Black KM, Bollinger BK, Botka AJ, French TL, Thompson TL, Schad VC, Greenstein JL, Gefter ML, Exley MA, Swain PA, Briner TJ (1996) Nat Med 2:1129
21. Landry DW, Yang GXQ (1997) J Addict Dis 16:1
22. Landry DW, Zhao K, Yang GXQ, Glickman M, Georgiadis TM (1993) Science 259:1899
23. Matsushita M, Hoffman TZ, Ashley JA, Zhou B, Wirsching P, Janda KD (2001) Bioorg Med Chem Lett 11:87
24. Cashman JR, Berkman CE, Underiner GE (2000) J Pharm Exp Ther 293,952:961
25. Yang G, Chun J, Arakawa-Uramoto H, Wang X, Gawinowicz MA, Zhao K, Landry DW (1996) J Am Chem Soc 118:5881
26. Kamendulis LM, Brzezinski MR, Pindel EV, Bosron WF, Dean RA (1996) J Pharmacol Exp Ther 279:713
27. Poet TS, McQueen CA, Halpert JR (1996) Drug Metab Dispos 24:74
28. Pan WJ, Hedaya MA (1999) J Pharm Sci 88:468
29. Sukbuntherng J, Martin DK, Pak Y, Mayersohn M (1996) J Pharm Sci 85:567
30. Browne SP, Slaughter EA, Couch RA, Rudnic EM, McLean AM (1998) Biopharm Drug Dispos 19:309
31. Carmona GN, Baum I, Schindler CW, Goldberg SR, Jufer R (1996) Life Sci 59:939
32. Lynch TJ, Mattes CE, Singh A, Bradley RM, Brady RO, Dretchen KL (1997) Toxicol Appl Pharmacol 145:363
33. Mattes CE, Lynch TJ, Singh A, Bradley RM, Kellaris PA, Brady RO, Dretchen KL (1997) Toxicol Appl Pharmacol 145:372
34. Mattes CE, Belendiuk GW, Lynch TJ, Brady RO, Dretchen KL (1998) Addict Biol 3:171
35. Lockridge O, Blong RM, Masson P, Froment M-T, Millard CB, Broomfield CA (1997) Biochemistry 36:786
36. Gately SJ (1991) Biochem Pharmacol 41:1249
37. Gately SJ, MacGregor RR, Fowler JS, Wolf AP, Dewey SL, Schlyer DJ (1990) J Neurochem 54:720
38. Darvesh S, Hopkins DA, Geula C (2003) Nature Rev Neurosci 4:131
39. Giacobini E (ed) (2003) Butyrylcholinesterase: its function and inhibitors. Dunitz Martin, Great Britain
40. Lerner RA, Benkovic SJ, Schultz PG (1991) Science 252:659
41. Jones RAY (1979) Physical and Mechanistic organic chemistry. Cambridge University Press, Cambridge

42. McMurry J (1988) Organic chemistry, 2nd edn. Cole, California
43. Lowry TH, Richardson KS (1987) Mechanism and Theory in organic chemistry, 3rd edn. Harper and Row, New York
44. Williams A (1987) In: Page MI, Williams A (eds) Enzyme mechanisms. Burlington, London, p 123
45. Li P, Zhao K, Deng S, Landry DW (1999) Helvetica Chim Acta 82:85
46. Zhan CG, Landry DW, Ornstein RL (2000) J Am Chem Soc 122:1522
47. Zhan CG, Landry DW, Ornstein RL (2000) J Am Chem Soc 122:2621
48. Zhan CG, Landry DW, Ornstein RL (2000) J Phys Chem A 104:7672
49. Bender ML, Thomas RJ (1961) J Am Chem Soc 83:4189
50. Bender ML, Matsui H, Thomas RJ, Tobey SW (1961) J Am Chem Soc 83:4193
51. Bender ML, Heck HA (1967) J Am Chem Soc 89:1211
52. Bender ML, Ginger RD, Unik JP (1958) J Am Chem Soc 80:1044
53. O'Leary MH, Marlier JF (1979) J Am Chem Soc 101:3300
54. Guthrie JP (1991) J Am Chem Soc 113:3941
55. Hengge A (1992) J Am Chem Soc 114:6575
56. Marlier JF (1993) J Am Chem Soc 115:5953
57. Sherer EC, Turner GM, Lively TN, Landry DW, Shields GC (1996) J Mol Model 2:62
58. Sherer EC, Yang G, Turner GM, Shields GC, Landry DW (1997) J Phys Chem A 101:8526
59. Sherer EC, Turner GM, Shields GC (1995) Int J Quantum Chem Quantum Biol Symp 22:83
60. Turner GM, Sherer EC, Shields GC (1995) Int J Quantum Chem Quantum Biol Symp 22:103
61. Fairclough RA, Hinshelwood CN (1937) J Chem Soc 538
62. Rylander PN, Tarbell DS (1950) J Am Chem Soc 72:3021
63. Zhan CG, Landry DW (2001) J Phys Chem A 105:1296
64. Becke AD (1993) J Chem Phys 98:5648
65. Lee C, Yang W, Parr RG (1988) Phys Rev B 37:785
66. Gonzalez C, Schlegel HB (1989) J Chem Phys 90:2154
67. Gonzalez C, Schlegel HB (1990) J Phys Chem 94:5523
68. Tomasi J, Persico M (1994) Chem Rev 94:2027
69. Cramer CJ, Truhlar DG (1996) In: Tapia O, Bertran J (eds) Solvent effects and chemical reactions. Kluwer, Dordrecht, p 1
70. Cramer CJ, Truhlar DG (1999) Chem Rev 99:2161
71. Chipman DM (1997) J Chem Phys 106:10194
72. Chipman DM (1999) J Chem Phys 110:8012
73. Schmidt MW, Baldridge KK, Boatz JA, Elbert ST, Gordon MS, Jensen JH, Koseki S, Matsunaga N, Nguyen KA, Su SJ, Windus TL, Dupuis M, Montgomery JA (1993) J Comput Chem 14:1347
74. Zhan CG, Bentley J, Chipman DM (1998) J Chem Phys 108:177
75. Zhan CG, Chipman DM (1998) J Chem Phys 109:10543
76. Zhan CG, Chipman DM (1999) J Chem Phys 110:1611
77. Zheng F, Zhan CG, Ornstein RL (2001) J Chem Soc Perkin Trans 2 2355
78. Zheng F, Zhan CG, Ornstein RL (2002) J Phys Chem B 106:717
79. Zhan CG, Dixon DA, Sabri MI, Kim MS, Spencer PS (2002) J Am Chem Soc 124:2744
80. Dixon DA, Feller D, Zhan CG, Francisco SF (2002) J Phys Chem A 106:3191
81. Zhan CG, Norberto de Souza O; Rittenhouse R, Ornstein RL (1999) J Am Chem Soc 121:7279
82. Zhan CG, Zheng F (2001) J Am Chem Soc 123:2835

83. Dixon DA, Feller D, Zhan CG, Francisco SF (2003) Int J Mass Spectrom 227:421
84. Zhan CG, Dixon DA, Spencer PS (2003) J Phys Chem B 107:2853
85. Zhan CG, Dixon DA, Spencer PS (2004) J Phys Chem B 108:6098
86. Chen X, Zhan CG (2004) J Phys Chem A 108:3789
87. Chen X, Zhan CG (2004) J Phys Chem A 108:6407
88. Xiong Y, Zhan CG (2004) J Org Chem 69:8451
89. Zhan CG, Deng SX, Skiba JG, Hayes BA, Tschampel SM, Shields GC, Landry DW (2005) J Comput Chem 26:980
90. Frisch MJ, Trucks GW, Schlegel HB, Scuseria GE, Robb MA, Cheeseman JR, Zakrzewski VG, Montgomery JA, Stratmann RE, Burant JC, Dapprich S, Millam JM, Daniels AD, Kudin KN, Strain MC, Farkas O, Tomasi J, Barone V, Cossi M, Cammi R, Mennucci B, Pomelli C, Adamo C, Clifford S, Ochterski J, Petersson GA, Ayala PY, Cui Q, Morokuma K, Malick DK, Rabuck AD, Raghavachari K, Foresman JB, Cioslowski J, Ortiz JV, Stefanov BB, Liu G, Liashenko A, Piskorz P, Komaromi I, Gomperts R, Martin RL, Fox DJ, Keith T, Al-Laham MA, Peng CY, Nanayakkara A, Gonzalez C, Challacombe M, Gill PMW, Johnson B, Chen W, Wong MW, Andres JL, Gonzalez AC, Head-Gordon M, Replogle ES, Pople JA (1998) Gaussian 98. Gaussian, Pittsburgh, PA
91. Gu Y, Kar T, Scheiner S (1999) J Am Chem Soc 121:9411
92. Meadows ES, De Wall SL, Barbour LJ, Fronczek FR, Kim MS, Gokel GW (2000) J Am Chem Soc 122:3325
93. Vargas R, Garza J, Dixon DA, Hay BP (2000) J Am Chem Soc 122:4750
94. Deng S, Bharat N, de Prada P, WLandry DW (2004) Org Biomol Chem 2:288
95. Mets B, Winger G, Cabrera C, Seo S, Jamdar S, Yang G, Zhao K, Briscoe RJ, Almonte R, Woods JH, Landry DW (1998) Proc Natl Acad Sci USA 95:10176
96. Nicolet Y, Lockridge O, Masson P, Fontecilla-Camps JC, Nachon F (2003) J Biol Chem 278:41141
97. Sun H, Yazal JE, Lockridge O, Schopfer LM, Brimijoin S, Pang YP (2001) J Biol Chem 276:9330
98. Sun H, Shen ML, Pang YP, Lockridge O, Brimijoin S (2002) J Pharmacol Exp Ther 302:710
99. Sun H, Pang YP, Lockridge O, Brimijoin S (2002) Mol Pharmacol 62:220
100. Zhan CG, Zheng F, Landry DW (2003) J Am Chem Soc 125:2462
101. Hamza A, Cho H, Tai HH, Zhan CG (2005) J Phys Chem B 109:4776
102. Bruice TC, Lightstone FC (1999) Acc Chem Res 32:127
103. Shurki A, Štrajbl M, Villá J, Warshel A (2002) J Am Chem Soc 124:4097
104. Masson P, Legrand P, Bartels CF, Froment M-T, Schopfer LM, Lockridge O (1997) Biochemistry 36:2266
105. Ekholm M, Konschin H (1999) J Mol Struct (THEOCHEM) 467:161
106. Harel M, Sussman JL, Krejci E, Bon S, Chanal P, Massoulie J, Silman I (1992) Proc Natl Acad Sci USA 89:10827
107. Masson P, Xie W, Froment MT, Levitsky V, Fortier PL, Albaret C, Lockridge O (1999) Biochim Biophys Acta 1433:281
108. Hu C-H, Brinck T, Hult K (1998) Int J Quantum Chem 69:89
109. Wlodek ST, Clark TW, Scott L, McCammon JA (1997) J Am Chem Soc 119:9513
110. Wlodek ST, Antosiewicz J, Briggs JM (1997) J Am Chem Soc 119:8159
111. Zhou HX, Wlodek ST, McCammon JA (1998) Proc Natl Acad Sci USA 95:9280
112. Malany S, Sawai M, Sikorski RS, Seravalli J, Quinn DM, Radic Z, Taylor P, Kronman C, Velan B, Shafferman A (2000) J Am Chem Soc 122:2981
113. Zhan CG, Gao D (2005) Biophys J 89:3863

114. Gao Y, Atanasova E, Sui N, Pancook JD, Watkins JD, Brimijoin S (2005) Mol Pharmacol 67:204
115. Gao D, Zhan CG (2006) Proteins 62:99
116. Gao D, Zhan CG (2005) J Phys Chem B 109:23070
117. Pan Y, Gao D, Yang W, Cho H, Yang GF, Tai HH, Zhan CG (2005) Proc Natl Acad Sci USA 102:16656
118. Gao D, Cho H, Yang W, Pan Y, Yang GF, Tai HH, Zhan CG (2006) Angew Chem Int Ed 45:653
119. Morris GM, Goodsell DS, Halliday RS, Huey R, Hart WE, Belew RK, Olson AJ (1998) J Comput Chem 19:1639
120. Zhang Y, Kua J, McCammon JA (2002) J Am Chem Soc 124:10572
121. Tai K, Shen T, Börjesson U, Philippopoulos M, McCammon JA (2001) Biophys J 81:715
122. Kua J, Zhang YK, Eslami AC, Butler JR, McCammon JA (2003) Protein Science 12:2675
123. Bernstein FC, Koetzle TF, Williams GJ, Meyer EF, Brice MD, Rodgers JR, Kennard O, Shimanouchi T, Tasumi M (1977) J Mol Biol 112:535
124. Rosenberry TL (1975) Proc Nat Acad Sci USA 72:3834
125. Alvarez-Idaboy JR, Galano A, Bravo-Pérez G, Ruíz ME (2001) J Am Chem Soc 123:8387